Received: 21 April 2022 | Accepted: 22 April 2022

DOI: 10.1002/gj.4480

RESEARCH ARTICLE

WILEY

Geochronology and petrogenesis of granitoids and associated mafic enclaves from Ghohroud in the Urumieh–Dokhtar Magmatic Arc (Iran): Evidence for magma mixing during the closure of the Neotethyan Ocean

Tayebeh Khaksar[1] | Nematollah Rashidnejad-Omran[1] | Shuang-Qing Li[2] | Shu-Guang Song[3] | Ali Kananian[4] | Fukun Chen[5] | Su Li[6]

[1]Department of Geology, Faculty of Basic Sciences, Tarbiat Modares University, Tehran, Iran

[2]Institut für Geowissenschaften, Universität Heidelberg, Heidelberg, Germany

[3]Department of Geology, School of Earth and Space Sciences, Peking University, Beijing, China

[4]School of Geology, College of Science, University of Tehran, Tehran, Iran

[5]Department of Geochemistry and Environmental sciences, School of Earth and Space Sciences, University of Science and Technology of China, Hefei, China

[6]State Key Laboratory of Geological Processes and Mineral Resources, Institute of Earth Science, Chinese University of Geosciences, Beijing, China

Correspondence
Shuang-Qing Li, Universität Heidelberg, Institut für Geowissenschaften, 69120 Heidelberg, Germany.
Email: lsq@ustc.edu.cn

Funding information
National Nature Science Foundation of China, Grant/Award Number: 41802047; TMU Research Grant Council

Handling Editor: E. Bozkurt

The Ghohroud granitoids (GG), containing mafic microgranular enclaves (MMEs) are located in the central part of the Urumieh-Dokhtar Magmatic Arc (UDMA) in central Iran. They are associated with the subduction-related magmatism in the Alpine-Himalayan orogenic belt. The GG are comprised of a variety of intermediate and felsic rocks, including tonalite, granodiorite, granite, diorite porphyry and monzodiorite. The MMEs are gabbroic diorite and tonalite in composition and characterized by a fine-grained hypidiomorphic microgranular texture with occasional chilled margins. They show rounded, sharp or irregular contact with the host granitoids. The occurrences of quartz, K-feldspar and corroded plagioclase indicate that MMEs are the products of mixing between mantle and crust-derived magmas. New ages of zircon U–Pb dating reveal that the GG in the Kashan area emplaced at ca. 19–17 Ma (Burdigalian). All the samples of MMEs and granitoid host rocks in this study are metaluminous and calc-alkaline with I-type affinities. They are enriched in light rare earth elements (LREEs) and show slight negative Eu anomalies ($Eu/Eu^* = 0.36–0.95$). These features in a combination with the relative depletion in Nb, Ta, Ti and P, indicate the granitoids and MMEs are closely associated with subduction-related magmas at an active continental margin. The host rocks yield relatively homogeneous isotopic compositions of initial $^{87}Sr/^{86}Sr$ ratios ranging from 0.706036 to 0.707055, $\varepsilon Nd(t)$ values varying from −2.25 to 0.8, and the Nd model ages (T_{DM}) vary in a limited range of 0.70–0.96 Ga. The MMEs show similar initial $^{87}Sr/^{86}Sr$ ratios (0.706420–0.707366), $\varepsilon Nd(t)$ values (−1.32 to −0.27), T_{DM} (0.68–1.09 Ga) and Pb isotopic compositions with host granitoids, which imply they attained isotopic equilibration during magma mingling and mixing. In combination with the petrographic, chemical and isotopic results, we suggest that the origin of MMEs and their host rocks were related to the interaction between crust-derived melts and mantle-derived mafic magmas. The magma-mixing event possibly occurred

during the transition from subduction to collision in the UDMA along with the closure of the Neotethyan ocean.

KEYWORDS
Ghohroud granitoids, Iran, mafic magmatic enclave (MME), magma mixing, Neotethyan, Urumieh–Dokhtar Magmatic Arc

1 | INTRODUCTION

The Zagros orogen, which is part of the Alpine–Himalayan orogenic belt in Iran, was formed by the continental collision between the Arabian and Eurasian plates in the Middle to Late Miocene (e.g., Agard, Omrani, Jolivet, & Mouthereau, 2005; Alavi, 1994, 2007; Dercourt et al., 1986; Mohajjel & Fergusson, 2014; Sen, Temel, & Gourgaud, 2004) following the northeastward subduction of Neotethys oceanic plate beneath the central Iranian continental crust during the Permo-Triassic (Agard et al., 2011; Berberian, Muir, Pankhurst, & Berberian, 1982; Shahabpour, 2007) or Cretaceous (e.g., Mohajjel & Fergusson, 2000). This orogenic belt is divided into three NW-SE trending parallel zones (Figure 1; Alavi, 2004; Mohajjel, Fergusson, & Sahandi, 2003): (a) Zagros Fold-and-Thrust Belt (ZFTB; Berberian & King, 1981), (b) Sanandaj-Sirjan Zone (SSZ; Stöcklin, 1968), and (c) Urumeih-Dokhtar Magmatic Arc (UDMA; Aftabi & Atapour, 2000; Alavi, 2004; Allen, Jackson, & Walker, 2004; Dilek, Imamverdiyev, & Altunkaynak, 2010; McClusky, Reilinger, Mahmoud, Ben Sari, & Tealeb, 2003). The ZFTB is formed by thrusting and folding successions of Palaeozoic to Mesozoic shelf deposits. The SSZ consists of Palaeozoic-Triassic metamorphic rocks, which are the main host of calc-alkaline plutonic bodies (e.g., Azizi, Chung, Tanaka, & Asahara, 2011; Hassanzadeh et al., 2008; Sepahi & Athari, 2006; Shahbazi et al., 2010). The UDMA, with a length of about 2,000 km

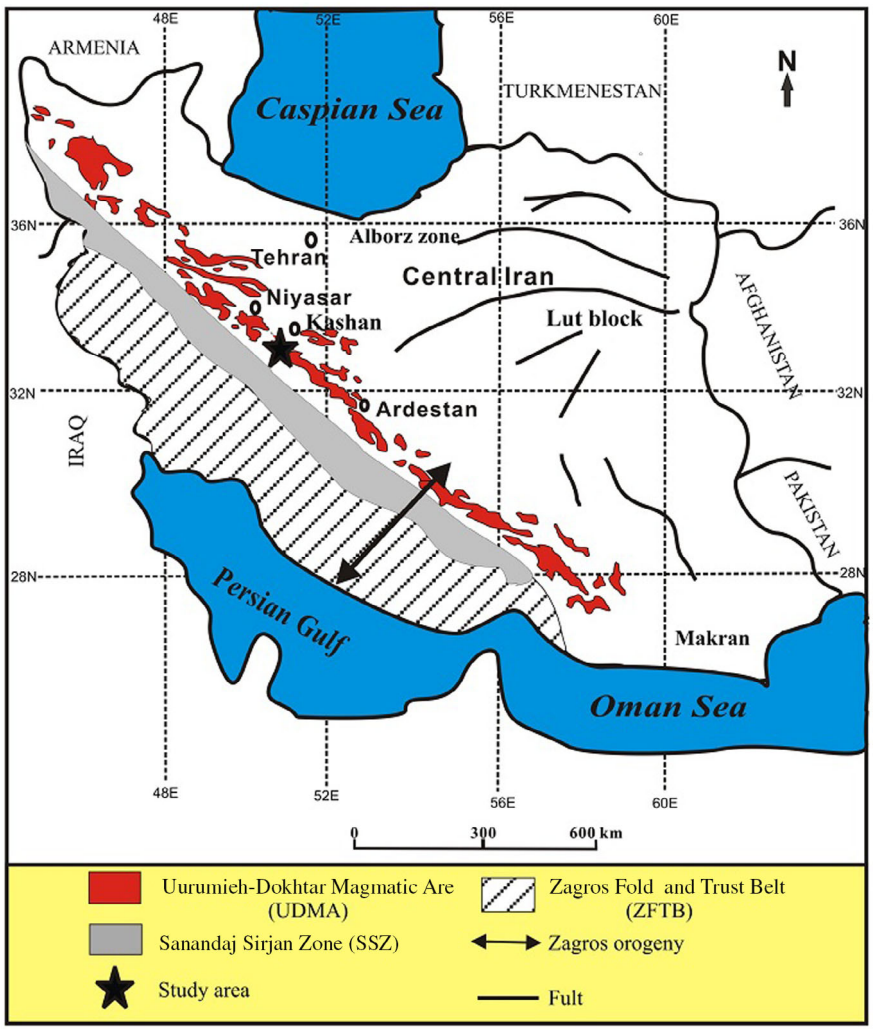

FIGURE 1 Simplified regional geological map of Iran showing the major tectonic units (modified after Alavi, 1994). Study area is shown by a dark star and is located in central Urumieh-Dokhtar Magmatic Arc

and a width of 100–150 km, is a broad belt of mostly Cenozoic magmatic rocks in the north of SSZ (e.g., Aftabi & Atapour, 2000; Alavi, 2004; Allen et al., 2004; Dilek et al., 2010; Emami, 1981; Mcclusky et al., 2003).

The linear volcano-plutonic complex developed in the UDMA has been considered as a magmatic arc formed by the subduction of the Neotethyan oceanic lithosphere beneath the Central Iranian Plate in Late Mesozoic and Cenozoic times (Alavi, 1991). The maximum magmatic flare-up in the UDMA occurred between the Eocene and Oligocene (e.g., Ghorbani, Graham, & Ghaderi, 2014; Kananian, Sarjoughian, Nadimi, Ahmadian, & Ling, 2014; Khaksar et al., 2020; Moghadam et al., 2016; Moghadam & Stern, 2011; Verdel et al., 2011).

There has been much debate about the origin of the magmatism in the UDMA, such as resulting from rift-related mantle upwelling (e.g., Amidi, Emami, & Michel, 1984; Amidi & Michel, 1985) or derivation associated with the subduction of Neotethyan plate beneath central Iran (e.g., Kananian et al., 2014; Rezaei-Kahkhaei, Galindo, Pankhurst, & Esmaeily, 2011; Sarjoughian et al., 2012; Sepidbar et al., 2019). Models of Island arc (e.g., Ghorbani, 2006; Shahabpour, 2007), slab break-off (Omrani et al., 2008), sub-continental lithospheric mantle delamination (Haschke, Ahmadian, Murata, & McDonald, 2010), and slab rollback (Verdel et al., 2011), post-collisional lithospheric shortening and asthenosphere upwelling (Asadi, 2018) have been suggested as favourite processes to build the UDMA magmatic rocks. With the deepening of research, it is generally believed that the closure of the Neotethyan Ocean had played a crucial role in the generation of igneous rocks in UDMA. According to previous studies, the magmatism in UDMA is dominated by volcanic rocks (Eocene to Oligocene; Chiu et al., 2013) that are composed of trachybasalt, andesite, basaltic andesite, ignimbrite and pyroclastic rocks (Ghorbani et al., 2014; Ghorbani & Bezenjani, 2011; Yeganehfar, Ghorbani, Shinjo, & Ghaderi, 2013). Fewer plutons including gabbro to granite (Oligo-Miocene; Berberian & Berberian, 1981) distribute sporadically throughout the UDMA (e.g., Haghipour & Aghanabati, 1985). They are predominantly calc-alkaline and tholeiitic in nature (e.g., Ahmadi & Posht Kuhi, 1993; Jung, Kursten, & Tarkian, 1976). The minor alkaline and shoshonitic rocks have been reported recently (e.g., Arvin, Pan, Dargahi, Malekizadeh, & Babaei, 2007; Dargahi, 2007; Omrani et al., 2008). The oldest rocks in the UDMA are calc–alkaline intrusive rocks that cut across Upper Jurassic formations and are overlying unconformably by lower Cretaceous fossiliferous limestones (e.g., Dargahi, Arvin, Pan, & Babaei, 2010).

It has been noted that the mafic microgranular enclaves (MMEs) with more mafic compositions than the host rocks were well preserved in calc-alkaline igneous rocks, including volcanics (e.g., Ban, Takahashi, Horie, & Toya, 2005; Clynne, 1999; Eichelberger, Cherkoff, Dreher, & Nye, 2000) and plutons (e.g., Chen, Chen, Li, & Wang, 2016; Didier, 1973; Didier & Barbarin, 1991; Fernández & Castro, 2018; Kumar & Rino, 2006; Sun et al., 2020; Vernon, 1984). The Ghohroud granitoids (GG) are located in the central part of UDMA and characterized by the presence of MMEs, which provides a unique opportunity to address the regional tectonic and magmatic processes. However, there are relatively few studies on geochronology and geochemistry of GG (Chiu et al., 2013; Ghasemi & Tabatabaei Manesh, 2015; Khaksar et al., 2020), which hindered the knowledge of regional tectono-magmatic evolution. In this study, we present a comprehensive dataset from petrographic characteristics to zircon U–Pb ages in addition to whole-rock chemistry and Sr–Nd–Pb isotopes of the MMEs and granitoid host rocks from UDMA. Our new data not only place constraints on the magmatic processes, and emplacement history of GG, but also provide significant insight into the evolution of magmatism which was tightly related to the Neotethyan closure.

2 | GEOLOGICAL BACKGROUND

The GG are located in the north of Isfahan. They are parts of the Kashan Igneous Complex in central UDMA (Khaksar et al., 2020) and cover an area of about 70 km^2 (Figure 2). In general, the study area can be subdivided into five major lithological units: (a) the major outcrops of sedimentary rocks including an Early Jurassic sequence composed of conglomerate, marl and limestone, which is termed as Shemshak Formation; (b) an Early Eocene sequence including siliceous tuff, shale, marl and limestone; (c) Late Eocene volcanic and pyroclastic rocks, including andesite, basalt and rhyolite; (d) Miocene nummulitic limestone sequence that locally transformed to marble and skarn; and (e) a sequence followed by Miocene volcanic rocks including andesite and dacite (age of ~14 Ma; Khaksar et al., unpublished data).

The GG are granular and less porphyritic in texture and fine-grained in the margin with a white to grey colour (Figure 3a). Based on field and petrographic observations, especially modal mineral characteristics, the GG consist of two groups of rocks including felsic rocks (granite, granodiorite, tonalite) and intermediate rocks (diorite porphyry and monzodiorite). Tonalite and granodiorite occupy about ~70% of the mass volume, while granite forms less than 10% of the volume. The diorite porphyry and monzodiorite masses are scattered as small outcrops throughout the southern part of the study area and never exceed 20% by volume. The contact relations between these units are transitional. Various degrees of contact metamorphism between the intrusions and the country rocks (Jurassic Shemshak Formation comprising shale and sandstone) led to the formation of fertile skarns and hornfels (Ahankoub, 2003). In some areas, the main intrusive bodies are intruded by felsic (dacite to rhyolite) and mafic-intermediate (diorite to basaltic andesite) dikes (Figure 3b). Both types are variable in thicknesses from a few centimetres to a few meters and generally display a northwest to southeast orientation, which follows the trend of the main regional fault in this area (NW-SE; Safaei, Taheri, & Vaziri-Moghaddam, 2008). The MMEs are mainly concentrated in the tonalite and granodiorite rocks and less frequently in some parts of the granite, diorite porphyry and monzodiorite. They are characterized by widespread and heterogeneous dispersion in the field. The MMEs are fine-grained compared to the host rocks and have irregular ellipsoidal shapes (~10–50 cm in diameter) and show sharp, rounded or irregular contacts with the host granitoids (Figure 3c). The MMEs are characterized by a microgranular-

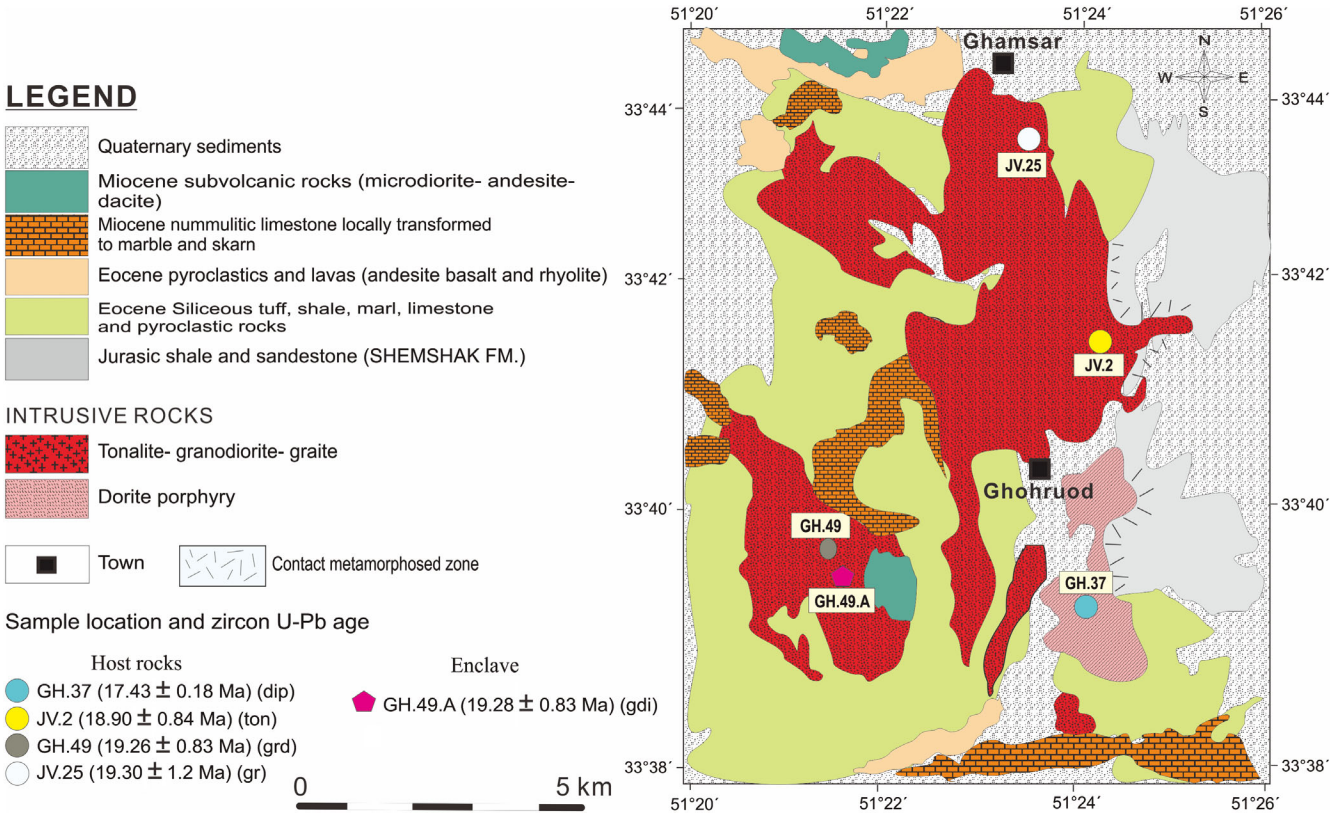

FIGURE 2 Simplified geological map of the Ghohroud granitoids (modified after Radfar, 1993). Localities of samples for zircon U–Pb dating in this study (GH.37 and GH.49.A) and literature data (JV.2, GH.49 and JV.25; Khaksar et al., 2020) are also shown. Abbreviation of rock types: dip, diorite porphyry; gr, granite; gbdi, gabbroic diorite; grd, granodiorite; ton, tonalite

hypidiomorphic texture and chilled margins, which may result from the mixing of magmas with different temperatures (Hibbard, 1991; Vernon, 1984; Zhao, Zhong, & Wang, 1994).

3 | ANALYTICAL METHODS

3.1 | Zircon U–Pb dating

Zircon grains for samples of enclave and host granitoid were concentrated using a procedure combining magnetic and heavy liquid methods and then selected by hand under a binocular microscope at the Geological Survey of Iran. The zircons were then mounted on adhesive tape, embedded in epoxy resin and polished to about half of their thickness. The U–Pb compositions of zircons were analysed by a laser ablation-inductively coupled plasma mass spectrometer (LA-ICP-MS). The analytical data are presented in Table S1. Measurements of U–Pb analysis for zircons were carried out on an Agilent-7500a quadrupole ICP-MS coupled with a New Wave SS UP193 laser sampler at the China University of Geosciences, Beijing. The laser spot size of 36 μm, the laser energy density of 8.5 J/cm^2 and a repetition rate of 10 Hz were applied for analysis. National Institute of Standards and Technology 610 glass and zircon standard 91500 (Wiedenbeck et al., 1995) were used as external standards, Si as the internal standard, and zircon standard Qinghu zircon as the secondary standard. The software GLITTER (ver. 4.4, Macquarie University) was used to process the isotopic ratios and element concentrations of zircons. The common lead correction was done following Anderson (2002). Age calculations and plots of Concordia diagrams were made using Isoplot/Ex v. 3.0 program (Ludwig, 2003). Analytical details are described in Song, Niu, Wei, Ji, and Su (2010).

3.2 | Whole-rock major and trace element analyses

Whole-rock major and trace element analyses were performed on five fresh samples from the GG, on the basis of careful petrographic observations. The samples were crushed in specially designed steel jaw crushers and then powdered in a tungsten carbide ball mill to a grain size of <200 mesh. The whole-rock major element oxides were analysed for some samples using a Leman Prodigy inductively coupled plasma optical emission spectroscopy (ICP-OES) at the China University of Geosciences, Beijing (CUGB). The analytical precisions (1σ) for most major elements on account of master standards GSR-1, GSR-3, GSR-5 (National geological standard reference materials of China) and USGS AGV-2 are better than 1% except TiO_2 (~1.5%) and P_2O_5 (~2.0%). Loss on ignition (LOI) was gained by placing 1 g of sample powders in the furnace at 1000°C for several hours before being cooled in a desiccator and reweighed.

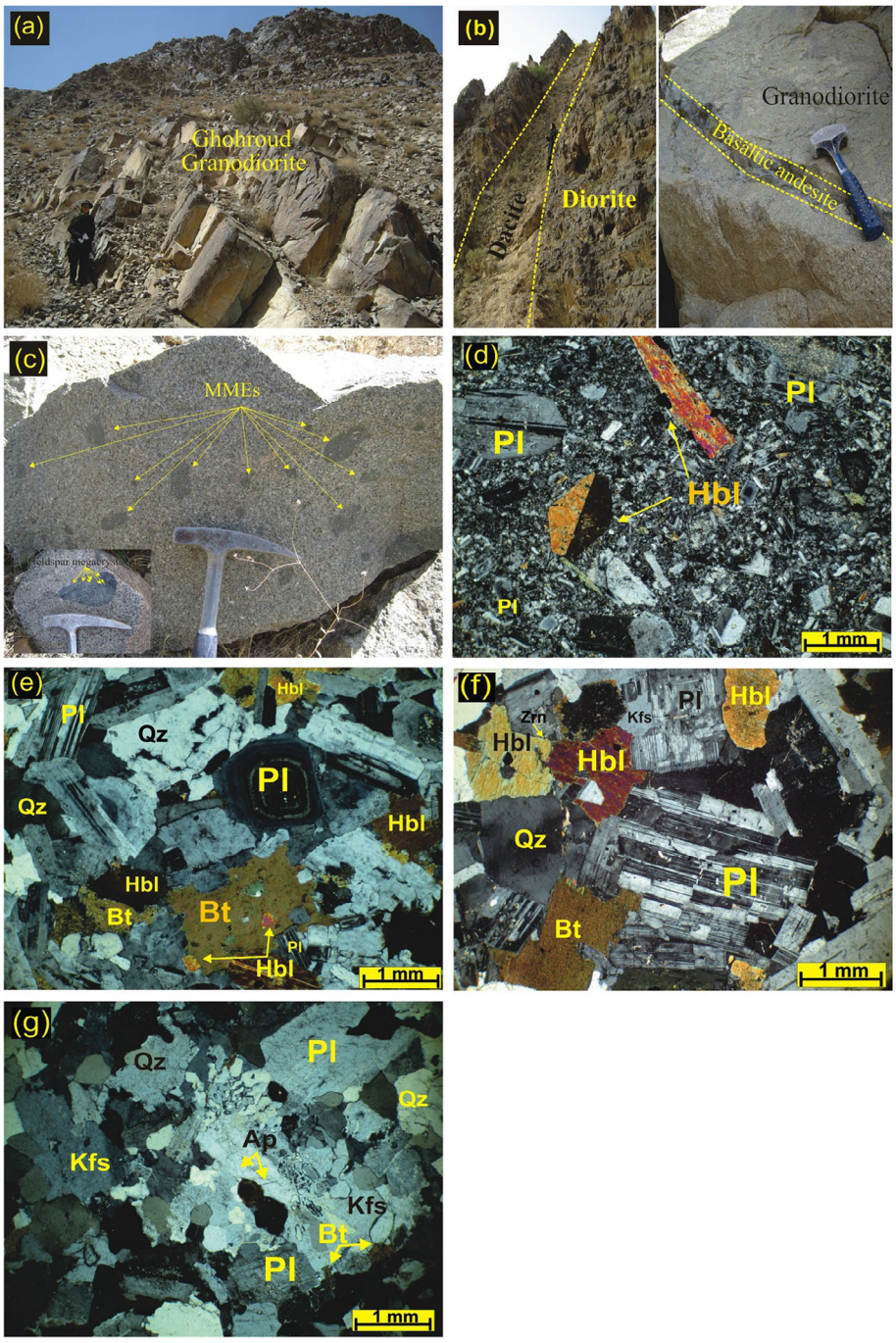

FIGURE 3 Field photos and thin section photomicrographs (in cross-polarized light) of the Ghohroud granitoids (GG): (a) outcrops of granodiorite in the southern sector of the GG; (b) dykes cutting the intrusions; (c) mafic microgranular enclaves (MMEs) enclosed by a granodiorite; (d) Hornblende phenocrysts exhibiting twining in diorite; (e–g) photomicrographs showing the main textures and mineral assemblages of the tonalite, granodiorite and granite, respectively. Mineral abbreviations are Bt, biotite; Hbl, hornblende; Kfs, Kfeldspar; Pl, plagioclase; Qz, quartz; Zrn, zircon

The trace element analyses were determined using an Agilent-7500a quadrupole ICP-MS in the Institute of Earth Science, CUGB. About 40 mg power of each sample was dissolved in a distilled acid mixture (1:1 HNO_3 + HF) by a Teflon digesting vessel and heated on a hotplate at 185°C for 48 hr using high-pressure bombs for digestion/dissolution. The sample was then evaporated to incipient dryness, prefixed with 1 ml 6N HNO_3, and heated again to incipient dryness. The sample was again dissolved in 2 ml of 3N HNO_3 in high-pressure bombs at 165°C for a further 24 hr to ensure complete dissolution. Such digested samples were finally diluted with Milli-Q water to a dilution factor of 2,000 in a 2% HNO_3 solution for analyses. Master standards (GSR-1, GSR-3, GSR-5 and USGS AGV-2) were used to monitor the analytical accuracy and precision. Analytical accuracy, as indicated by a relative difference between measured and recommended values, is better than 5% for most elements, and 10–15% for Cu, Zn, Gd, and Ta.

3.3 | Sr–Nd–Pb isotopic measurements

In this study, the whole-rock Sr–Nd isotope analyses were performed by two different methods. Some samples were analysed by multi-

collector inductively coupled plasma mass spectrometer method (MC-ICP-MS) at MOE Key Laboratory of Orogenic Belts and Crustal Evolution, Peking University. In this method, about 300 mg of the unknown sample and ~200 mg of the standard sample of Basalt-Columbia-River (BCR-2) were dissolved in HF + HNO_3 in Teflon vessels and heated at 140°C for 7 days in order to be completely dissolved. The pure Sr and Nd were separated from the remaining solution by passing through conventional cation columns (AG50W and P507). The $^{87}Rb/^{86}Sr$ and $^{147}Sm/^{144}Nd$ ratios were calculated based on Rb, Sr, Sm, and Nd contents determined by ICP-MS (CUGB). Mass fractionation corrections for Sr and Nd isotopic compositions were normalized to $^{86}Sr/^{88}Sr = 0.1194$ and $^{146}Nd/^{144}Nd = 0.7219$, respectively. Rock standard BCR-2 was used to evaluate the separation and purification process of Rb, Sr, Sm, and Nd. Repeated analyses for the Nd and Sr standard samples (JNdi and NBS987) yielded $^{143}Nd/^{144}Nd = 0.512197 \pm 11$ (2σ) and $^{87}Sr/^{86}Sr = 0.710229 \pm 11$ (2σ), respectively. For other samples, the Sr–Nd–Pb isotopic analyses were carried out at the Key Laboratory of Crust–Mantle Materials and Environments of CAS at the University of Science and Technology of China (USTC), Hefei, according to the methods of Chen, Li, Wang, Li, and Siebel (2007). Whole-rock Sr and LREE were isolated on quartz columns by ion-exchange chromatography with a 5-ml resin bed of AG 50W-X12, 200–400 mesh. Nd was separated from other LREEs on quartz columns using 1.7-ml Teflon powder coated with HDEHP, di(2-ethylhexyl)-orthophosphoric acid, as a cation exchange medium. Pb was leached from the solutions and then purified twice through AG1-x8 resin. Sr, Nd, and Pb isotopic measurements were carried out on a Finnigan MAT-262 thermal ionization mass spectrometer. Sr was loaded with a Ta-HF activator on preconditioned Ta filaments. Nd was loaded as phosphate on preconditioned Re filaments. $^{143}Nd/^{144}Nd$ ratios are normalized to $^{146}Nd/^{144}Nd = 0.7219$, and $^{87}Sr/^{86}Sr$ ratios to $^{86}Sr/^{88}Sr = 0.1194$ using a Rayleigh fractionation law. During the course of this study, analyses of the JNd-1 reference solution yielded $^{143}Nd/^{144}Nd = 0.512118 \pm 0.000012$ (2 *SD*, $n = 2$) and NIST 987 yielded $^{87}Sr/^{86}Sr$ ratios of 0.710246 ± 0.000012 (2 *SD*, $n = 4$). Measured Pb isotopic ratios were corrected for thermal mass fractionation using a value of 0.11% per atomic mass unit as has been inferred from the analysis of the reference material NIST 981.

4 | RESULTS

4.1 | Petrographic features

4.1.1 | Granitoid rocks

The rocks of the GG mainly consist of quartz, plagioclase, amphibole, biotite and minor K-feldspar. Most rocks from the GG are coarse- to medium-grained and granular to porphyritic in texture (Figure 3d–g). These rocks are composed of euhedral to subhedral plagioclase crystals with oscillatory zoning and sieve textures (Figure 3e), and subhedral to euhedral or prismatic amphibole in a finer-grained matrix containing plagioclase, quartz, K-feldspar, amphibole, biotite, pyroxene and iron–titanium oxides (Figure 3d) with decreasing abundance. Some plagioclase crystals show oscillatory zoning and the hornblendes in some samples are characterized by a twining texture (Figure 3e). Plagioclase and hornblende appear as phenocrysts in diorite porphyries and hornblende is the most common mafic mineral in these rocks with higher abundances than that in granitic, granodioritic and tonalitic rocks (Figure 3d). In some samples, large phenocrysts of

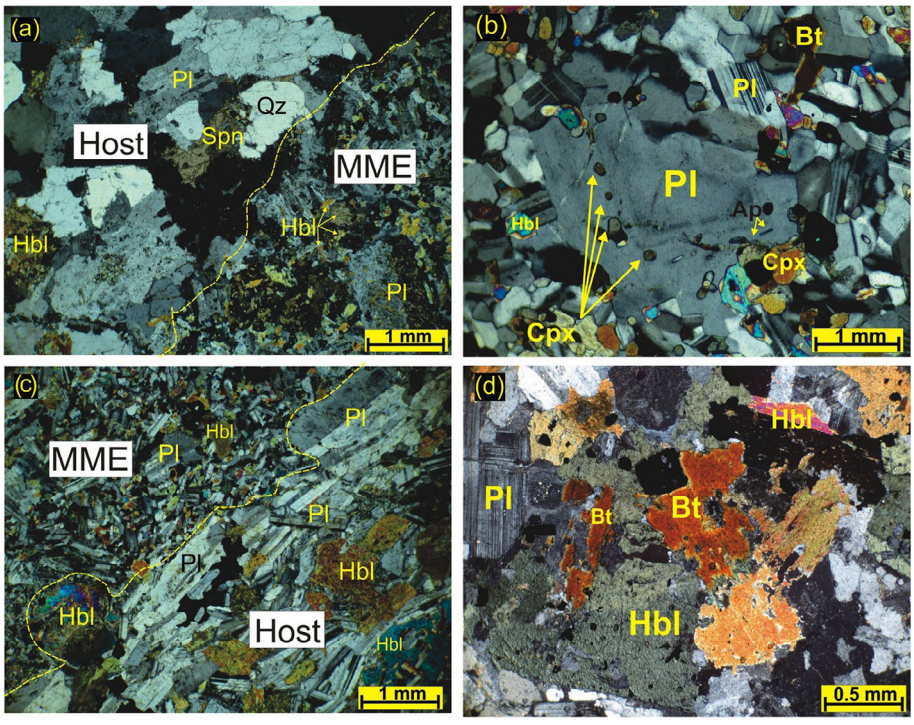

FIGURE 4 (a) Photomicrographs showing textural relationships between the granitoid host rocks and their enclaves; (b) Plagioclase phenocrysts embedded in a medium- to a fine-grained matrix (in mafic microgranular enclaves [MMEs], cross-polarized); (c) large plagioclases and mafic phases crosscut the enclave-host boundary; (d) mafic clot in the MME (cross-polarized light). Mineral abbreviations are the same as in Figure 3, except Cpx, clinopyroxene

plagioclase contain hornblende and/or apatite inclusions. Sometimes the small plagioclase crystals were enclosed by alkali feldspar as inclusions. Plagioclase occasionally has been replaced by sericite and epidote. Hornblende encloses fine-grained plagioclase and minor opaque and shows twining texture in some minerals (Figure 3d–f). Some hornblende grains have locally altered to actinolite, chlorite and titanite, especially along crystal rims. Biotite forms large subhedral to euhedral crystals. They are present as brown flanks that have been occasionally replaced by chlorite at rims in granitic rocks (Figure 3e–g). Micrographic and granophyric intergrowth textures are common in granitic rocks (Figure 3g). The quartz crystals are usually clustered and surrounded by alkali feldspar. Magnetite, zircon and apatite are accessory phases. Calcite, chlorite, epidote and sericite are secondary minerals in all rock types. Zircons usually occur as prismatic crystals.

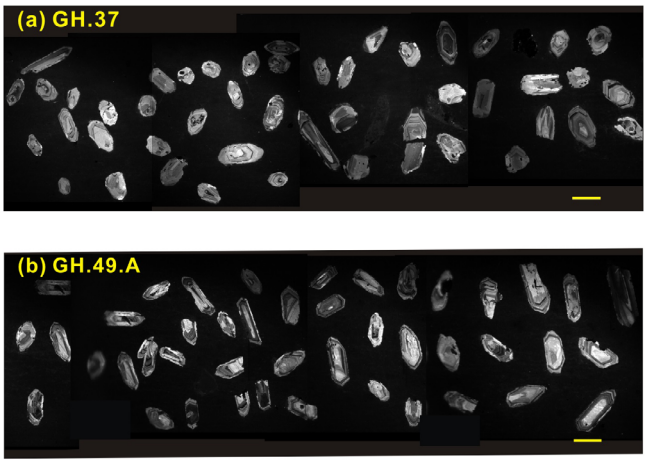

FIGURE 5 Cathodoluminescence images of typical zircon grains in samples of diorite (a), and gabbroic diorite (b). The yellow bars are 200 μm long

4.1.2 | Magmatic microgranular enclaves

The MMEs are fine-grained and gabbroic diorite and tonalite in composition. They are dark-coloured, agglomerated globular or elliptical and show massive structures with various sizes from several to tens of millimetres (Figure 3c). The samples of MMEs usually show chilled margins and distinct contacts with the host granitoids (Figure 4a), some of them rarely show gradual boundaries with the host rocks. These MMEs are characterized by porphyritic textures with small anhedral plagioclase phenocrysts embedded in a medium- to fine-grained matrix composed of pyroxene, plagioclase, K-feldspar, quartz, biotite and hornblende (Figure 4b). Most plagioclase crystals are subhedral to anhedral, showing rounded/corroded and zoned features. In some cases, large plagioclases and mafic phases cross-cut the enclave-host boundary (Figure 4c). Oscillatory zoning in plagioclase is also common in enclaves and hosts. The most abundant mafic mineral is pyroxene followed by amphibole. Some pyroxenes are partly replaced by amphiboles and occur as relics in the core of amphibole grains. Amphibole is more abundant than biotite in the enclaves. The amphiboles are variably sized crystals of single prismatic or acicular hornblende. Amphibole crystals occasionally occur as mafic clots (Figure 4d). Biotites usually accompany amphiboles. Quartz and K-feldspar crystals are characterized by interstitial growth filling the interstices between plagioclase and mafic minerals. Accessory minerals of the enclaves include zircon and acicular apatite. Occasionally, several amphibole and biotite show alterations to chlorite and iron oxides.

4.2 | Zircon U–Pb ages

Two samples from the GG were selected for LA-ICP-MS zircon U–Pb dating (Table S1 and Figure 6). They include one sample of diorite porphyry (GH.37) for the host rock and a gabbroic diorite sample (GH.49.

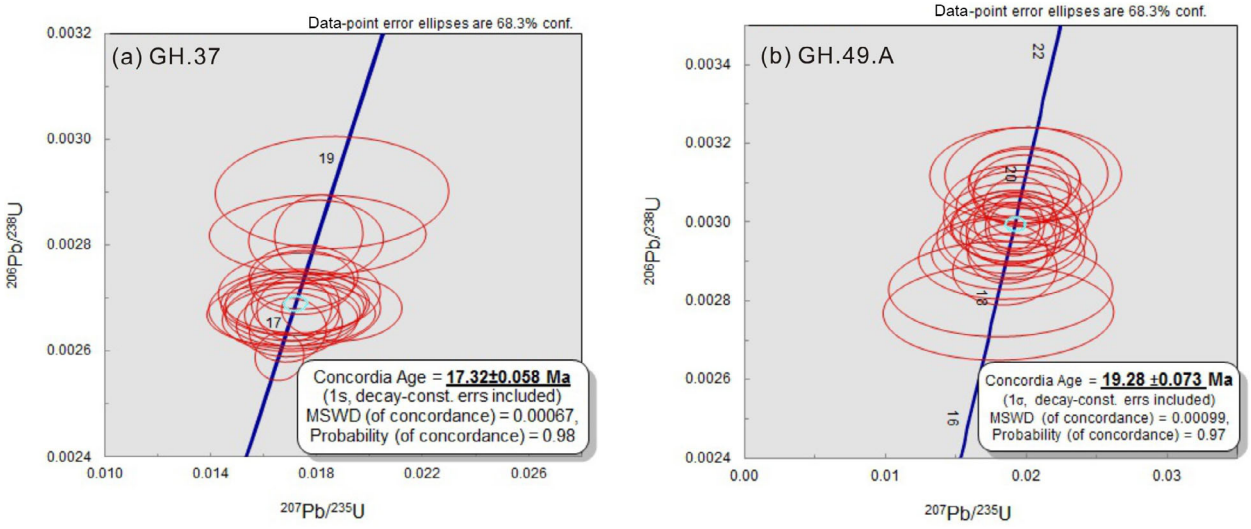

FIGURE 6 Concordia diagrams for zircons from the samples of the host GG (a) and MME (b). See text for detailed discussions

A) for the MMEs. The results of the other three samples including tonalite (JV.2), granodiorite (GH.49), and granite (JV.25) of the Kashan igneous complex were selected for comparison (Khaksar et al., 2020). The locations of the samples are shown in Figure 2. The errors in individual analyses are cited as 2σ. The zircon crystals are short to long prismatic with variable lengths from ~100 to ~300 μm. Most of the zircon grains showed weak to moderate magmatic oscillatory zoning in cathodoluminescence (CL) images (Figure 5).

From the diorite porphyry sample (GH.37), 28 grains were measured of which 25 grains are concordant and yielded an average mean $^{206}Pb/^{238}U$ age of 17.32 ± 0.058 Ma (Burdigalian; Figure 6a). Three grains are discordant and along with an array with the mean age as a lower intercept. The acquired age is consistent with the results of surrounding plutons, which show ages of about 19 Ma (Khaksar et al., 2020). The GH.49.A was taken from gabbroic dioritic enclaves and 26 analyses of zircon grains yielded a Concordia age of 19.28 ± 0.21 Ma (Burdigalian; Figure 6b).

4.3 | Major and trace element geochemistry

To understand the petrogenesis and relationship of the host granitoids and entrained mafic enclaves better, the results of this study and our previous research are jointly addressed. Geochemical data of the samples from the GG and literature data of Kashan plutons for comparison (Khaksar et al., 2020) are listed in Table S2. In the classification diagram of Middlemost (1994), the samples of host rocks plot mainly in the fields of diorite, monzonite to monzodiorite, tonalite, granodiorite, and granite, whereas the MMEs plot in the fields of gabbroic diorite and tonalite (Figure 7a). The results are compatible with Quartz-Alkali feldspar-Plagioclase (QAP) modal classification diagram (Streckeisen, 1976; Figure 7b). The host rocks have SiO_2 and MgO contents of 56.05–73.72 wt% and 0.54–5.41 wt%, respectively, whereas the associated MMEs show lower SiO_2 of 52.47–63.73 wt%, but higher MgO of 2.98–5.07 wt%. All samples have a sub-alkaline affinity, which belongs to the calc–alkaline series (Figure 7c). The host

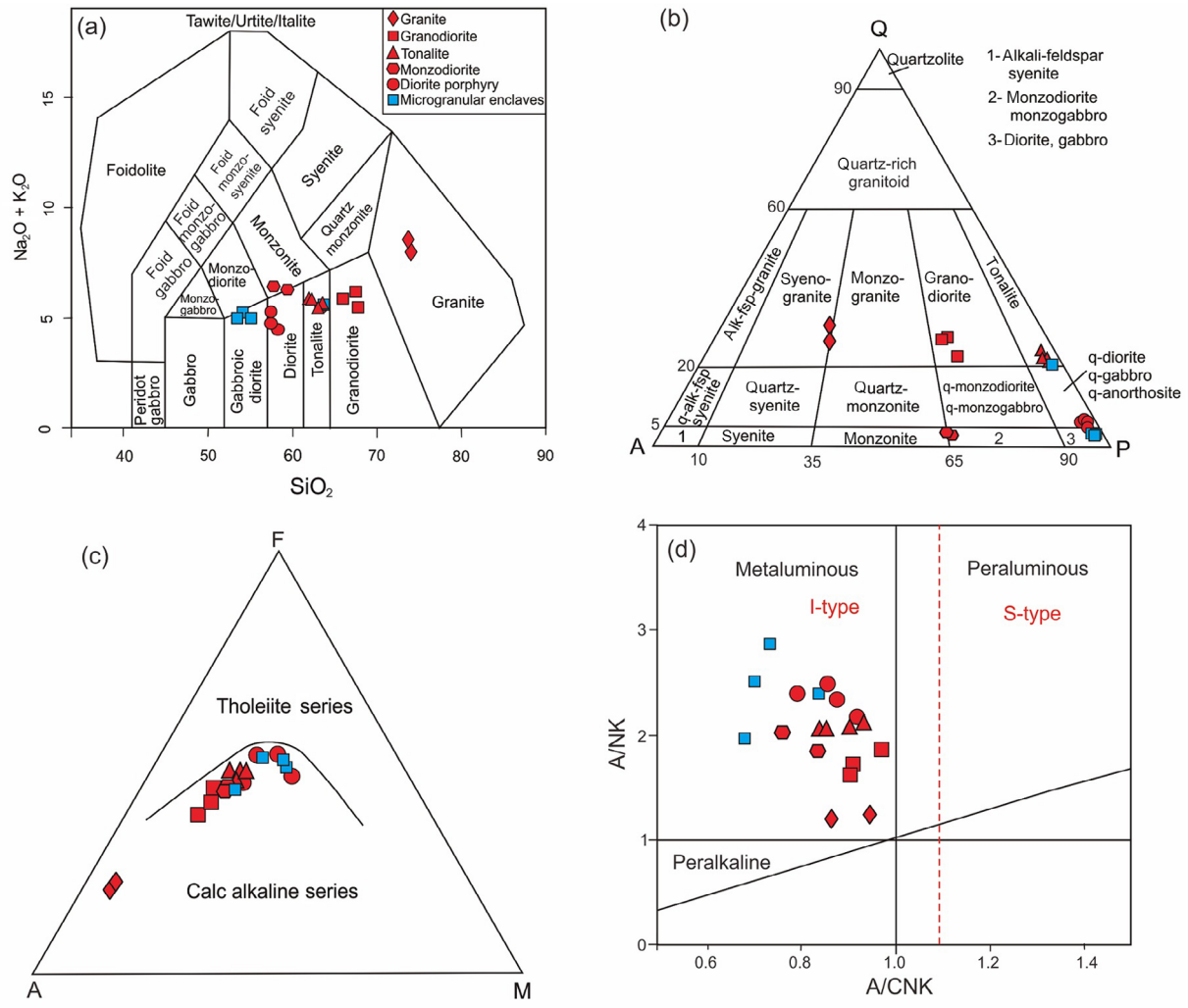

FIGURE 7 (a) Classification diagram (Middlemost, 1994) Chemical classification R1 versus R2 diagram (De la ruche et al., 1980) distinguish mafic to felsic compositions for the GG; (b) QAP diagram (Streckeisen, 1976); (c) AFM diagram (Irvine & Baragar, 1971) for identification of tholeiitic- and calc-alkaline affinities of the samples from the studied area; (d) A/NK versus A/CNK diagram [ANK = molar $Al_2O_3/(Na_2O + K_2O)$ and ACNK = molar $Al_2O_3/(CaO + Na_2O + K_2O]$ (Shand, 1943)

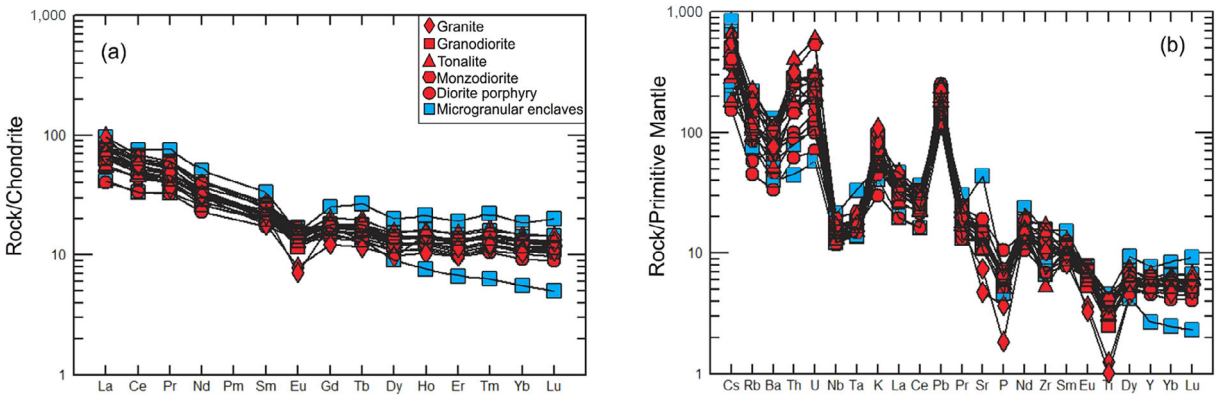

FIGURE 8 (a) Chondrite-normalized rare earth element patterns (Nakamura, 1974), and (b) Primitive mantle-normalized trace element patterns (Sun & McDonough, 1989) for selected samples of the Ghohroud granitoids (GG) and mafic magmatic enclaves. Data of GG are from Khaksar et al. (2020) except sample GH.37. Symbols are the same as in Figure 7

rocks and MMEs are metaluminous with aluminum saturation index [ASI=molar $Al_2O_3/(CaO + K_2O + Na_2O)$] ranging from 0.79 to 0.96 (Host) and 0.66 to 0.83 (MMEs), which confirms their I-type affinities (Figure 7d).

In the Chondrite-normalized REE patterns (Figure 8a; Nakamura, 1974), all samples show similar shapes with moderate enrichment in LREEs ($La_n/Yb_n = 3.51–17.49$), flat heavy rare earth elements (HREEs; $Gd_n/Yb_n = 1.11–3.11$) and significant negative Eu anomalies ($Eu/Eu^* = 0.36–0.95$). In the primitive mantle-normalized multi-element patterns (Figure 8b; Sun & McDonough, 1989), all samples are characterized by enrichment in large-ion lithophile elements (LILE; e.g., Cs, K, U, Th, Pb) and pronounced depletion in the incompatible high-field-strength elements (HFSEs) such as Nb, Ti and Ta (and P) relative to the primitive mantle. The MMEs display minor depletions in P and Ti and lower concentrations of Ba, Th and Zr compared to those of the host rocks.

4.4 | Whole-rock Sr–Nd and Pb isotopes

Eight samples were selected for Sr–Nd and Pb isotopic analyzes. The studied samples cover the whole bulk-rock compositional spectrum present in the study area ranging from diorite to granite as well as two samples of MMEs. The $^{87}Sr/^{86}Sr$ and $^{143}Nd/^{144}Nd$ isotopic ratios for representative samples are presented in Table S3. The host rocks of the GG display relatively similar isotopic compositions of initial $^{87}Sr/^{86}Sr$ (0.706036–0.707055), initial $^{143}Nd/^{144}Nd$ (0.512500–0.512618) and $\varepsilon Nd(t)$ (−2.25 to 0.8), which were calculated at the age of ca. 19 Ma. The corresponding Nd model ages (T_{DM}; Depaolo, 1981) vary in a limited range of 0.70–0.96 Ga. Compared to the host rocks, the MMEs show similar isotopic compositions. Their initial $^{87}Sr/^{86}Sr$ range from 0.706420 to 0.707366 and $\varepsilon Nd(t)$ vary from −1.32 to −0.27 (Figure 9a). The Nd model ages of the MMEs are more scattered but range from 0.68 to 1.09 Ga.

Lead isotopic data for the GG are presented in Table S4. The studied samples are homogeneous in lead isotopic compositions. For the host granitoids, the measured $^{206}Pb/^{204}Pb$, $^{207}Pb/^{204}Pb$, and $^{208}Pb/^{204}Pb$ values are 19.00–19.08, 15.69–15.71, and 39.04–39.17, respectively. The associated MMEs show more consistent $^{206}Pb/^{204}Pb$, $^{207}Pb/^{204}Pb$, and $^{208}Pb/^{204}Pb$ values of 19.00–19.05, 15.69–15.70, and 39.08–39.09, respectively (Figure 9b).

5 | DISCUSSION

5.1 | Origin of microgranular enclaves

MMEs as a key for understanding the genesis of the magmatism are well developed in the Cenozoic granitoids within the UDMA (e.g., Gharamohammadi & Kananian, 2016; Kazemi, Kananian, Xiao, & Sarjoughian, 2018; Sarjoughian et al., 2012). The MMEs have relatively low silica content and relatively high Mg# (45.3–54.6), suggesting the contribution of a mantle-derived component for their generation. It has been suggested that the MMEs were refractory solid residues of partial melting in the source region (Chappell et al., 1987; Chappell & White, 1974). This type of enclave usually has coarse-grained texture and/or heterogeneous microstructures and is characterized by Al-rich minerals (such as sillimanite, garnet, etc.). The enclaves are often enclosed in S-type granitoids of older ages than their hosts (Vernon, 2014). However, the MMEs from the UDMA are fine-grained with poikilitic–equigranular to microporphiritic textures. They show sharp contacts with the host rocks and are characterized by chilled margins, oscillatory zoning and the absence of Al-rich minerals (garnet, cordierite, sillimanite, etc.). Thus, the MMEs of the UDMA should not have resulted from residues after partial melting.

The MMEs mafic enclaves can also be derived from country rocks as xenoliths that are entrained by the ascent magma in the magma chamber or through a conduit (e.g., Bonin, 2004; Didier, 1991; Didier & Barbarin, 1991; Maas, Kinny, Williams, Froude, & Compston, 1992; Yang, Wu, Chung, Wilde, & Chu, 2004, 2006). In this case, the enclaves usually have different ages of crystallization and geochemical characteristics compared to their host rocks. However,

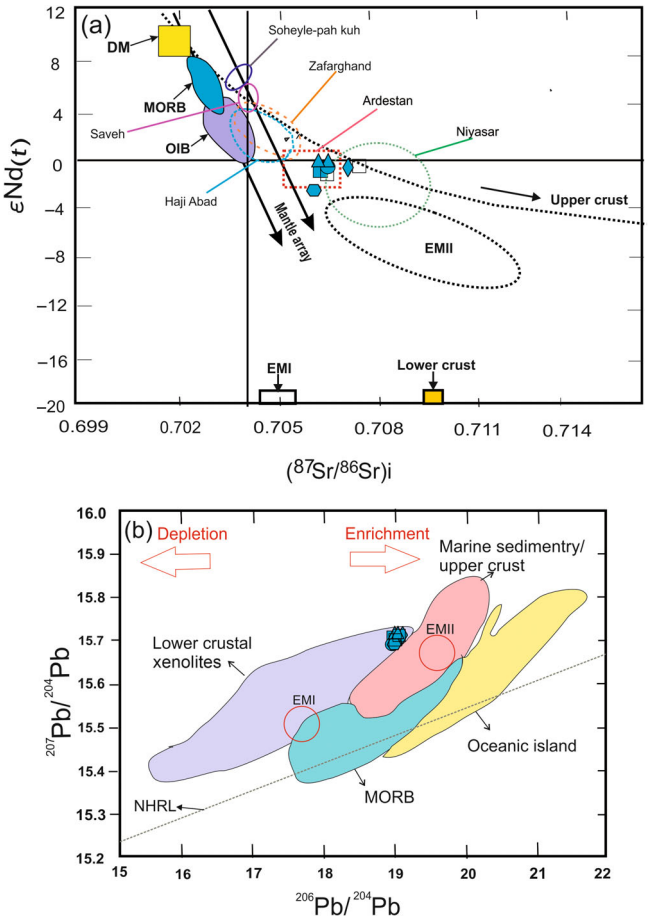

FIGURE 9 (a) ($^{87}Sr/^{86}Sr$)i versus $\varepsilon Nd(t)$ diagram. Reference data sources: MORB, mid-ocean ridge basalt; DM, depleted mantle; OIB, ocean-island basalt after Zindler and Hart (1986), EM I and EM II represent two types of mantle end-members, respectively (Hou, Zhang, Pan, & Yang, 2011). The lower crust values are from Ben Othman, Fourcade, and Allegre (1984); (b) Plots of $^{206}Pb/^{204}Pb$ versus $^{207}Pb/^{204}Pb$ for the selected samples from the Ghohroud granitoids. The data of fields of the upper crust and lower crust were taken from Bonev, Dilek, Hanchar, Bogdanov, and Klain (2011), and fields of Mid Ocean Ridge Basalt (MORB) and Ocean Island Basalt (OIB) are after Rollinson (1993). Symbols are the same as in Figure 7

the gabbroic diorite enclaves from GG show similar zircon U–Pb ages and Sr–Nd–Pb isotopic compositions with the host granodiorites and tonalites (Figures 6 and 9), indicating the MMEs were not xenoliths carried by the felsic host melts.

Another important mechanism involved in the genesis of MMEs is the mixing of mantle-derived and crustal melts (Barbarin, 2005; Didier & Barbarin, 1991; Silva, Hartmann, McNaughton, & Fletcher, 2000). For the samples of MMEs contained in GG, their spherical and ellipsoidal shapes (Figure 3c) indicate globules of mafic melts that were mingled with the felsic host melts (Lowell & Young, 1999; Yang et al., 2015), which is further supported by the plagioclase with absorbed margins (Figure 4b). In addition, the appearances of K-feldspar and plagioclase megacrysts as well as entrained feldspar and quartz in the MMEs, suggest a hybrid system formed by mixing of two end-member magmas with distinct compositions (e.g., Barbarin, 1990; Hibbard, 1991; Yang et al., 2015). Some phenocrysts of plagioclase and mafic phases lie across the boundary of the MMEs and the host rocks (Figure 4c), suggesting that low rheological contrasts between two magmas allow these phenocrysts transferred between the host granitoid magma and the mafic magma during the mixing when they still behaved as liquids at depths (e.g., Perugini, Poli, Christofides, & Eleftheriadis, 2003; Waight, Maas, & Nicholls, 2000). Furthermore, the chilled margins in some MMEs indicate significant contrasts in both temperature and viscosity between the two end-member melts of mixing. The interaction between the relative mafic magma and the felsic magma will induce rapid cooling and a high nucleation rate of the MME components. Therefore, the MMEs from UDMA were probably formed by a process of magma mixing based on their petrological relationships and similar geochemical compositions with their host rocks.

5.2 | Petrogenesis of the GG

The Ghohroud rocks have a wide compositional and lithological variation from gabbroic diorite to granite with metaluminous, I-type and subduction-related calc-alkaline affinities (Figure 7). There are several petrogenetic models involved to explain the compositional variation of I-type intrusive rocks: (a) fractional crystallization (b) magma mingling or mixing (c) melt extraction from restate or un-melted source material (d) wall-rock assimilation and (e) combinations of previous processes (Chappell, 1996). Chappell and White (1974) suggested that I-type granitoids were most probably generated by partial melting of mafic to intermediate meta-igneous crustal rocks. However, many researchers have also purposed that I-type granitoids may result from mixing between melts derived from crustal materials and mantle-derived melts (e.g., Fang et al., 2017; Kemp et al., 2007).

Based on geochemical data as discussed above, the samples from the GG show depletion of Nb and Ti and enrichment in LILEs and LREEs (Figure 8), which suggest typical features of crustal melts. However, these characteristics can also result from partial melting of an enriched mantle, which was metasomatized by fluids prior to melting (Cameron et al., 2003; Rottura et al., 1998). The host rocks in the Ghohroud have SiO_2 content >56 wt% and their Al_2O_3 content (13–17.46 wt%) is not consistent with basic parent melts in equilibrium with a mantle source (Al_2O_3 <15 wt%). Furthermore, the volume of diorite porphyry intrusions is much lesser than that of the tonalite and granodiorite (Figure 2), so it appears unlikely that felsic magmas were derived from mantle melts through fractional crystallization or assimilation-fractional crystallization processes, otherwise, abundant mafic rocks should be expressed. Experimental studies have shown that less silicic melts can result from a high degree of partial melting in the lower crust (Rapp & Watson, 1995). In addition, Ghasemi and Tabatabaei Manesh (2015) have proposed that the initial magma of the Ghohroud complex could result from the partial melting of the lower crust protoliths (amphibolite). In the Zr/Sm versus Nb/Tb (Figure 10a; Foley et al., 2002) and molar Al_2O_3/(MgO + FeOt; AFM)

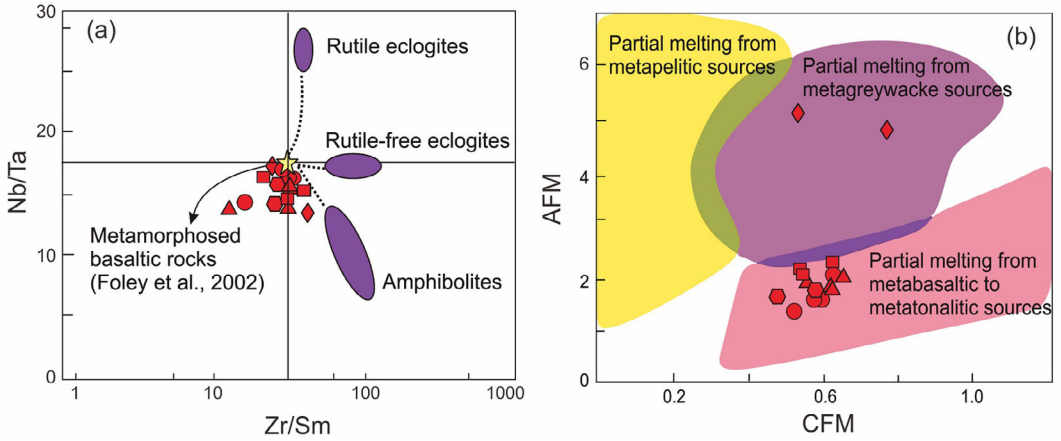

FIGURE 10 (a) Zr/Sm versus Nb/Tb diagram (Foley, Tiepolo, & Riccardo, 2002), displaying similarities between metamorphosed basaltic rocks and the Ghohroud granitoids. The horizontal and vertical lines represent chondritic Nb/Ta and Zr/Sm ratios of 17.6 and 25, respectively; (b) Molar Al_2O_3/(MgO + FeOt; AFM) versus molar CaO/(MgO + FeOt; CFM) diagram (modified from Altherr, Holl, & Hegner, 2000). Data source and symbols are the same as in Figure 7

versus CaO/(MgO + FeOt; CFM) diagrams (Altherr et al., 2000; Figure 10b), all of the GG sample plots in the metamorphosed basaltic rocks field, except for granitic samples (Figure 10b) which plot on the field of 'greywacke-derived melts' (the greywacke composition is the same as basic and intermediate rocks). These features indicate that contribution from the lower crust played a major role in the generation of the GG. Moreover, the linear variations in the diagrams of Zr/Nb versus Zr (Figure 11a) and La/Sm versus La (Figure 11b) suggest processes of partial melting are relevant during granitoid magma formation.

However, to some extent, fractional crystallization should also be involved in the evolution of magma, which is evidenced by geochemical compositions of the granitoids rocks. The decreasing Al_2O_3, MgO, CaO, Fe_2O_3tot and Sr contents and increasing K_2O and Ba contents along with increasing SiO_2 concentrations could be related to amphibole and calcic plagioclase fractionations (Figure 11c–i). The proportions of CaO, Fe_2O_3tot and MgO decrease with increasing SiO_2 may also reflect pyroxene fractionation. Negative Eu anomalies suggest that plagioclase was an important fractionating phase (Figure 8a). However, the weak correlations between $(^{87}Sr/^{86}Sr)_i$ or $\varepsilon Nd(t)$ and SiO_2 content (Figure 11j, k), suggests crustal assimilation is not a predominant petrogenetic process during the emplacement of the magma in the crust.

Critical trace elements ratios are indicative of different source characteristics of igneous rocks. The Rb/Sr ratios of the continental crust (0.12–0.22; Rudnick & Fountain, 1995; Wedepohl, 1995) are generally higher than the mantle-derived rocks (0.01–0.1; Hofmann, 1988; Taylor & McLennan, 1985). The average ratios of Nb/La, Nb/Ce, and $(La/Sm)_N$ in the crust are about 0.46, 0.23, and 4.25, respectively (Weaver & Tarney, 1984), but in the mantle are about 1.01, 0.39, and 1 (Sun & McDonough, 1989), respectively. In addition, mantle-derived rocks have low Th/Ta ratios of about 2, while the continental crust has a relatively high Th/Ta ratio of about 7 (Shellnutt, Wang, Zhou, & Yang, 2009). In this study, the Nb/La, Nb/Ce, Rb/Sr and $(La/Sm)_N$ ratios of the GG samples fall within ranges of 0.31–0.68, 0.16–0.36, 0.05–0.90 and 2.16–5.70, respectively, which indicate involvements of both mantle and lower crust components in the genesis of these granitoids. The GG show relative high values of Mg# (31.63–55.03; Mg/[Mg + Fe] * 100). At the same SiO_2 contents, the Mg# values are higher than the results of experimental magmas, which were generated by partial melting of the mafic lower crust. On the other hand, it has been suggested that the igneous rocks with Mg# values higher than 40 are usually generated by partial melting of mantle-derived components (Patino-Douce, 1999; Rapp, Watson, & Miller, 1991). Hence, mantle-derived components were necessary for the generation of the Ghohroud rocks which were suggested and related to the mixing of melts both from mantle and crust (e.g., Wang et al., 2004; Xu, Shinjo, Defant, Wang, & Rapp, 2002). This is further supported by the obvious mixing trend of two primitive magmatic end members for samples of GG and MMEs (Schiano, Monzier, Eissen, Martin, & Koga, 2010) in the diagrams of Rb/V versus Rb (Figure 12a) and Rb/V versus 1/V (Figure 12b).

Additionally, the isotopic compositions of GG also support their derivation from a hybrid source. The GG samples exhibit high initial $^{87}Sr/^{86}Sr$ and intermediate initial $^{143}Nd/^{144}Nd$ ratios. In the $\varepsilon Nd(t)$ versus $(^{87}Sr/^{86}Sr)_i$ diagram (Figure 9a), all samples plot to the right of the domain of the so-called 'mantle array'. They show $(^{87}Sr/^{86}Sr)_i$ and εNd values similar to mafic granulite terrains or massifs from the lower crust (Rudnick, 1992) that have been tectonically emplaced in the upper crust. The MMEs show generally $(^{87}Sr/^{86}Sr)_i$ values close to or in the range of that for the respective host granitoids, suggesting the MMEs and host granitoids attained isotopic equilibration during magma mingling and mixing (e.g., Barbarin, 2005; Fourcade & Javoy, 1991; Stephens, Holden, & Henney, 1991; Figure 9a). We added in the Figure (9a), some available literature data from the other plutons in the central UDMA during Eocene to Miocene compared with GG, in order to evaluate similarity or difference in the Nd–Sr compositions, source of magma and the evolution of magmatism in the central UDMA. As shown in the $\varepsilon Nd(t)$ versus $^{87}Sr/^{86}Sri$ diagram

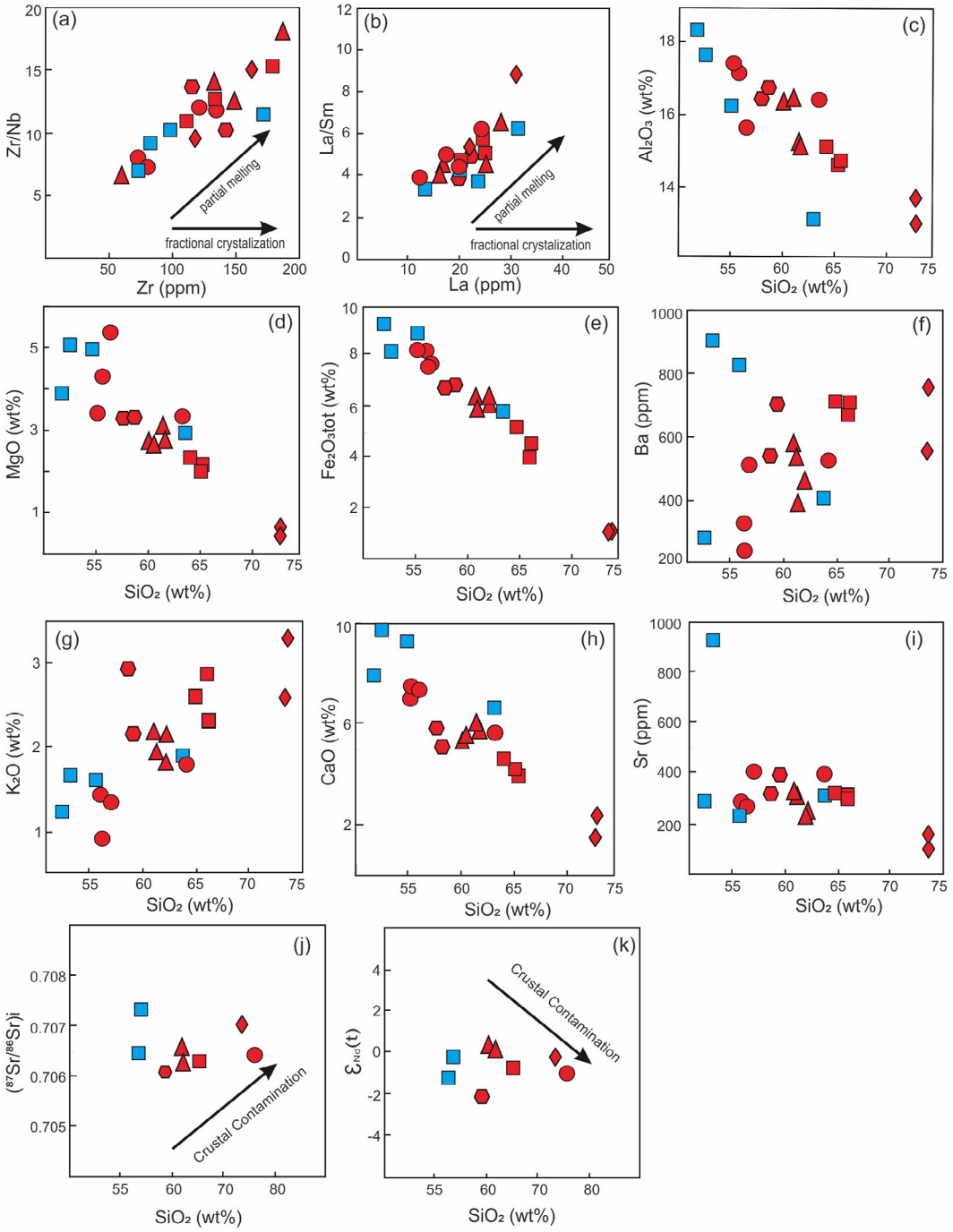

FIGURE 11 (a) Zr versus Zr/Nb, and (b) La versus La/Sm diagrams showing partial melting trend of the Ghohroud granitoids (GG) (after Allègre & Minster, 1978); (c–i) are Harker variation diagrams for samples from the GG; (j,k) SiO_2 versus $^{87}Sr/^{86}Sr(t)$ and $\varepsilon Nd(t)$ plots of the Ghohroud samples. Data source and symbols are the same as in Figure 7

(Figure 9a), all of the GG samples plotted close to the Eocene–Miocene Niyasar (Honarmand et al., 2014) and Oligocene- Miocene Ardestan (Babazadeh et al., 2017) with Nd–Sr isotope compositions similar to these plutons. While, the GG samples are different from those of the Middle Eocene Haji Abad (Kazemi et al., 2018), Late Oligocene Zafarghand (Sarjoughian, Lentz, Kananian, Ao, & Xiao, 2018), and Early Miocene granitoids from Natanz (Haschke et al., 2010) with same to higher $^{87}Sr/^{86}Sri$ and lower $\varepsilon Nd(t)$ values. These authors proposed that these granitoids resulted from interaction between mantle-derived melt and continental crust. The isotopic similarity of the GG to these plutonic rocks (Figure 9a) implies that these rocks were likely derived from a similar magma source. The Niyasar plutonic complex was suggested to be originated from the lithospheric mantle with characteristics of EM II during subduction of the Neotethyan oceanic slab. The geochemical and isotopic data indicate a mixed mantle–crustal origin of the middle Miocene granitoids, which

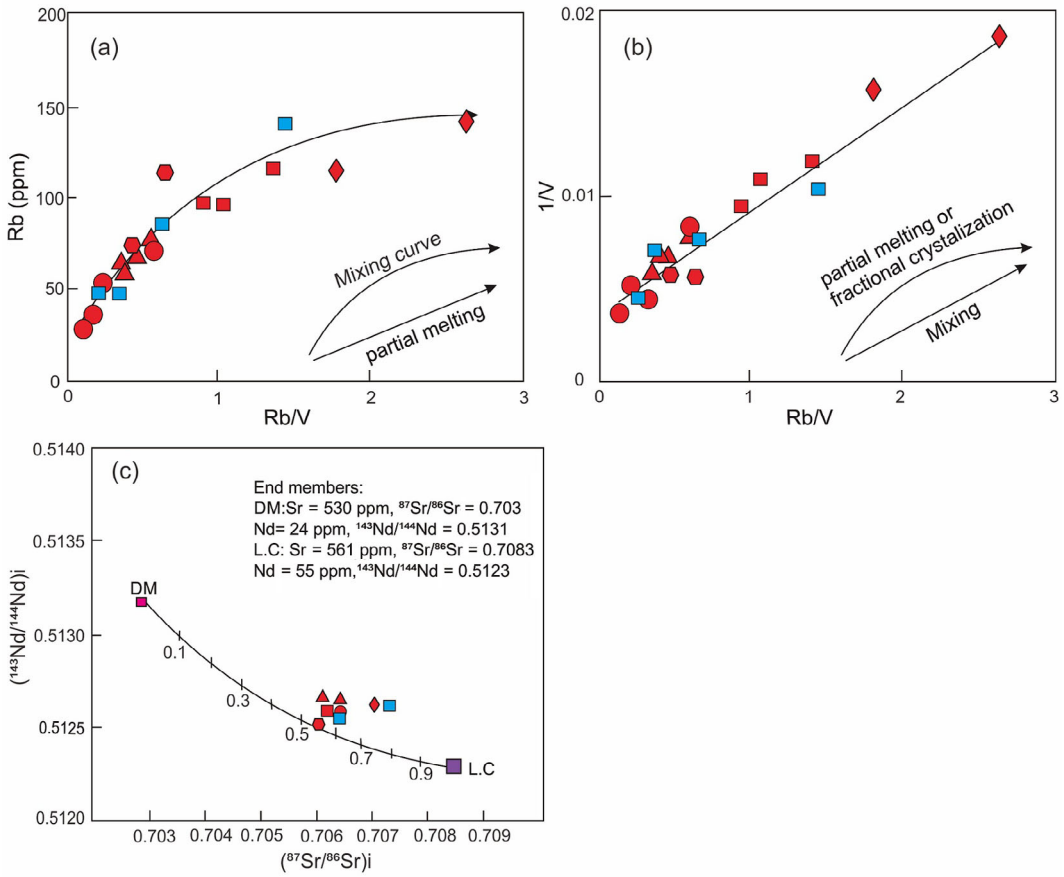

FIGURE 12 (a) Rb/V versus Rb and (b) Rb/V versus 1/V petrogenetic discrimination diagrams for the samples of the Ghohroud granitoids (Schiano et al., 2010); (c) a simple modelling diagram showing Sr–Nd isotopic variations because of magma mixing. LC: lower crust; DM: depleted mantle. Data source and symbols are the same as in Figure 7

consisted of ~60–70% lower crust-derived melt and ~30–40% mantle-derived melt, in a post-collision extensional setting (Honarmand et al., 2014). In addition, Babazadeh et al. (2017) suggested that south Ardestan plutonic rocks resulted from a mixture of ~6% crustal rocks and 94% mantle-derived melt based on the whole-rock Sr–Nd isotopic compositions. Moreover, the GG host rocks and MMEs yield Nd model ages ranging from 700 to 960 Ma and 680 to 1,090 Ma, respectively. These results support that they were derived from various degrees of mixing of magmas from the lower crust (Shafaii Moghadam et al., 2015) and lithospheric mantle (Figure 9a). The GG samples are homogeneous in lead isotopic compositions and generally subparallel to the Northern Hemisphere Reference Line (NHRL; Hart, 1984), and plot between the fields of EM I and EM II (closer to the field of EM II), indicating the igneous rocks were generated from mixing of materials from the lower crust and EM II. It is noteworthy that the GG data show a tendency of involvement of marine sediments, indicating modification of the magma source by the subduction (Figure 9b).

A simple model of mixing has been employed to reveal the proportions of mantle and crust components involved in the generation of the GG and associated MMEs (Figure 12c). In this model, two end-members are assumed to represent the average parent magma from the depleted mantle and lower continental crust. All samples plot on a mixing line between the end-members of the depleted mantle and lower crust, confirming the magma mixing process (Figure 12c). The isotopic ratios of Eastern Pontides are used as end-member for the modelling (Karsli et al., 2010 and references therein) since the compositions of the lower crust component for the study area are unknown. Eventually, the diagram indicates that the GG could be produced by mixing ~65–80% of lower crust-derived magma and ~20–35% of the mantle-derived mafic magma.

Based on the petrological and geochemical evidence as discussed above, we suggest that the parental magma of the GG was generated most likely from the mixing of mafic magma derived from the lithospheric mantle and lower crust-derived felsic melts in a convergent margin setting (Pearce, 1996). During the underplating and ascent of high-temperature mantle-derived basaltic magma, the lower continental crust could be partially melted which induced the generation of felsic melt. Consequently, the interaction between the melts derived from the lower crust and mantle-derived magmas at depths led to the formation of the extensive hybrid magmas. Finally, along with the migration of the hybrid magmas, various degrees of crystal fractionation in upper crustal levels would result in the development of granitoids with different compositions, ranging from diorite to granite, in the Ghohroud area. Furthermore, the similarities of ages and isotopic

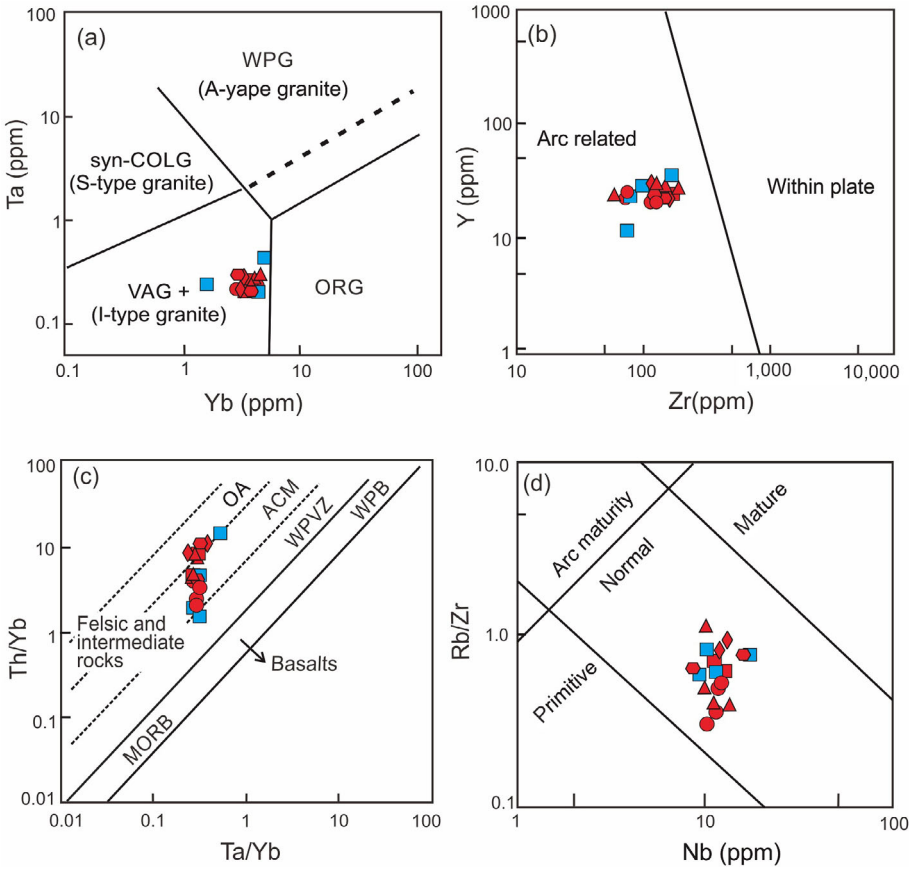

FIGURE 13 (a) Tectonic discrimination diagrams after Pearce et al. (1984), I-, S-, and A-type granites are from Christiansen and Keith (1996); (b) Y versus Zr geotectonic discrimination diagram for within-plate and from arc-related granites (after Müller & Groves, 1997); (c) Ta/Yb versus Th/Yb diagram (after Gorton & Schandl, 2000); (d) Nb versus Rb/Zr arc maturity discrimination diagram (after Brown, Thorpe, & Webb, 1984). Syn-COLG, syn-collision granites; VAG, volcanic arc granites; WPG, withinplate granites; ORG, ocean ridge granites. Symbols are the same as in Figure 7

compositions of the Miocene igneous rocks from a broad area of central UDMA corroborate contributions and interactions of continental crust and mantle melts for the arc magmatism during Neotethyan subduction.

5.3 | Tectonic implications

The tectonic evolution and magmatism of the UDMA are related to the subduction of the Neotethyan oceanic crust beneath the Central Iranian Microcontinent. The Tertiary magmatism in UDMA shows geochemical features comparable to those of Andean or Cordilleran type active continental margins such as the Eastern Pontides in Turkey or the Sierra Nevada plutons in the United States (Dewey, Pitman, Ryan, & Bonnin, 1973). The GG shows some features typical related to an active continental margin such as the presence of amphibole with accessory minerals (zircon, apatite, titanite and magnetite), the absence of aluminosilicate minerals (muscovite, garnet, andalusite, sillimanite and cordierite), and in particular, the presence of MMEs. These are pronounced features of amphibole-rich calc-alkaline granitoids associated with a subduction-related, active continental margin with mixed origin (Barbarin, 1999). In addition, a negative slope from LILE (Cs, Ba, Th, K, and U) to HFSE (Zr, Nb, Ti, and Hf) on the primitive mantle normalized spider diagram for the GG samples indicate their I-type features and association with active continental margin (Barbarin, 1999; Pearce, Harris, & Tindle, 1984). As shown in Figure 13a, the GG samples plot on the Ta versus Yb diagram (Pearce et al., 1984) in the volcanic arc granite (VAG) field. On the Zr versus Y (Müller & Groves, 1997) and Ta/Yb versus Th/Yb (Gorton & Schandl, 2000) diagrams, the GG samples fall in the arc-related and active continental margin fields (Figure 13b,c), which is consistent with the UDMA (e.g., Ayati, Yavuz, Asadi, Richards, & Jourdan, 2013; Berberian & King, 1981; Kananian et al., 2014; Moinvaziri, 1985; Mohajjel et al., 2003; Sarjoughian et al., 2012; Verdel et al., 2011). In the Rb/Zr versus Nb diagram (Brown et al., 1984), the samples of GG are plotted in the field of the normal continental arc (Figure 13d).

Based on the previous geochronological studies on the plutons in the central part of UDMA, Tertiary calc-alkaline magmatism developed during the Neotethyan subduction at ca. 53–17 Ma (Babazadeh et al., 2017; Chiu et al., 2013; Honarmand, Rashidnejad Omran, Corfu, Emami, & Nabatian, 2013; Shahsavari Alavijeh, Rashidnejad-Omran, & Corfu, 2017). According to Chiu et al. (2013), the majority of the calc-alkaline magmatism of Miocene occurred in the central and southern part of UDMA. A change of geochemical features of the magmatism from calc-alkaline to adakitic affinities has been noticed, which is consistent with the collision between Arabian and Eurasian plates in the southeastern part of UDMA. They suggested that the termination of arc magmatism took place progressively from the northwest to the southeast of UDMA, which was related to the diachronous collision between Arabia and Eurasia along the Zagros belt. In addition, the adakitic magmatism of the Middle Miocene (ca. 16 Ma; in Kashan) attributed to the collision-related crustal thickening, was considered

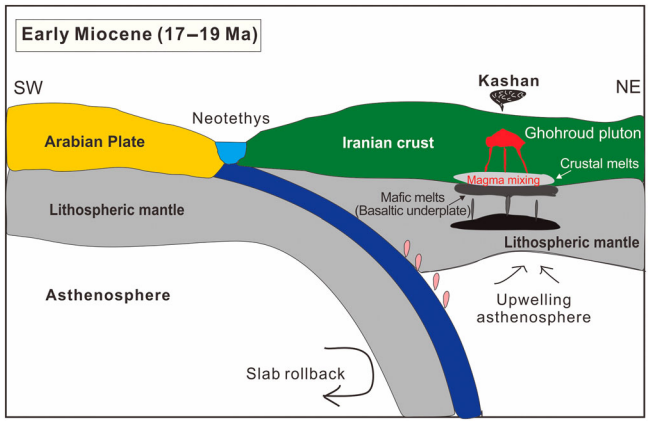

FIGURE 14 Schematic model showing the geodynamic evolution of the Early Miocene magmatism including widespread granitoids and related mafic magmatic enclaves in the central Urumieh-Dokhtar Magmatic Arc

as the ending of the arc activities in the central UDMA (Chiu et al., 2013). Honarmand et al. (2013) suggested that Miocene granitoids in the Niyasar magmatic segment related to post-collisional magmatism. The results of these studies indicated that the age of calc-alkaline magmatism and the timing of continental collision stepped down to the southeastward of the UDMA.

The majority of the magmatism in the UDMA, especially in its central and southern parts is Early Miocene in age (Berberian & Berberian, 1981; Chiu et al., 2013 and present study). Although the peak of the igneous activity (dominantly volcanism) lies in the Eocene–Oligocene, the plutonism in the Kashan area was more intensive in the Early Miocene periods. Omrani et al. (2008) argued for a magmatic quiescence in the UDMA from the Oligocene to the Early Miocene. They concluded that Arabia started colliding with Eurasia at this time and suggested that the younger magmatism of Neogene was related to a process of break-off of the subducted slab and sequent thermal re-equilibration in a post-collisional tectonic setting. On the other hand, Ghorbani et al. (2014) suggested that the Oligocene-Miocene basaltic magmatism in the central part of UDMA is related to the upwelling of the asthenospheric mantle, which might be prompted by or accompanied by a process of slab rollback. Further, they argued that the concomitant adakitic magma of Miocene also resulted from the slab rollback process.

Compared to the results of other calk-alkaline plutons in the UDMA, the magmatism related to the subduction of the Neotethyan must have started in the Early Eocene, and lasted until at least Early Miocene. In addition, the magmatism evolution in the Kashan area indicates the final stages of closure of the Neotethyan ocean occurred in the Miocene, involving change from subduction to the collision between the Arabian and Eurasian blocks. Based on the zircon U–Pb ages of ca. 17–19 Ma (Burdigalian) obtained for the pre-collisional GG in this study, it is reasonable to suggest that the Arabian–Eurasian continental collision related to the closure of the Neotethyan Ocean most likely happened after the Early Miocene. According to the geochronological, geochemical, and isotopic results of the MMEs and host rocks, the following scenario for the Early Miocene magmatism in central UDMA can be resumed. During the Early Miocene, prior to the collision between the Eurasian and Arabian blocks, rollback of the Neotethyan subducting slab triggered lithospheric extension and asthenospheric upwelling as well as decompression melting of the fertilized upper mantle, which was chemically enriched in incompatible components derived from the previous subducting slab. The underplating of the mantle-derived melts into a hot crust would have caused partial melting in the lower crust. Then, the interaction between the lower crust-derived melt and the magma derived from the lithospheric mantle formed a mixed magma, which subsequently ascended to shallower crustal levels. The heterogeneous hybrid magma further evolved into widespread granitoids with well-preserved MMEs (Figure 14).

6 | CONCLUSIONS

The following conclusions can be drawn from the results of field observation, petrography, geochemistry, and U–Pb dating in this study:

1. According to petrographic characteristics and whole-rock geochemical compositions, the GG mainly consist of diorite, monzodiorite, tonalite, granodiorite, granite and MMEs that show metaluminous, I-type and calc-alkalic affinities.
2. The field and petrographic features of MMEs in granodiorites and tonalites such as spherical and ellipsoidal outlines and chilled margins, as well as acicular apatites, oscillatory-zoned plagioclases and resorbed plagioclase megacrysts with poikilitic textures, indicate the mixing of coexisting mafic and felsic magmas.
3. Petrographic, geochemical and isotopic characteristics suggest a hybrid source of mixing of the lower crust and enriched mantle for the primary magmas of GG in an active continental margin.
4. New zircon U–Pb ages reveal that the emplacement of the GG in the Kashan area took place at ca. 17–19 Ma. In combination with the calc-alkaline affinities and pre-collisional signatures, the Early Miocene plutons in the UDMA were suggested to be developed during the transition from subduction to continental collision along with the closure of the Neotethyan Ocean, which further indicates the initiation of the Arabian-Eurasian continental collision no earlier than this period.

ACKNOWLEDGEMENTS

This study is based on the first author's PhD thesis at Tarbiat Modares University (TMU), Tehran, Iran between 2015 and 2018. Field studies were funded by the TMU Research Grant Council. This study was financially supported by the National Nature Science Foundation of China (Grants 41802047). Thoughtful and constructive comments by two anonymous reviewers substantially improved the manuscript.

CONFLICT OF INTEREST

The authors declare no potential conflict of interest.

PEER REVIEW

The peer review history for this article is available at https://publons.com/publon/10.1002/gj.4480.

DATA AVAILABILITY STATEMENT

The data that supports the findings of this study are available in the supplementary material of this article.

ORCID

Nematollah Rashidnejad-Omran https://orcid.org/0000-0003-3537-6692
Shuang-Qing Li https://orcid.org/0000-0002-2100-2414
Shu-Guang Song https://orcid.org/0000-0002-0595-7691
Ali Kananian https://orcid.org/0000-0001-5136-2130

REFERENCES

Aftabi, A., & Atapour, H. (2000). Regional aspects of shoshonitic volcanism in Iran. *Episodes*, *23*, 119–125.

Agard, P., Omrani, J., Jolivet, L., & Mouthereau, F. (2005). Convergence history across Zagros (Iran): Constraints from collisional and earlier deformation. *International Journal of Earth Sciences*, *94*, 401–419. https://doi.org/10.1007/s00531-005-0481-4.

Agard, P., Omrani, J., Jolivet, L., Whitechurch, H., Vrielynck, B., Spakman, W., … Wortel, R. (2011). Zagros orogeny: A subduction-dominated process. *Geological Magazine*, *148*, 692–725. https://doi.org/10.1017/S001675681100046X.

Ahankoub, M. (2003). *Mineralogical and geochemical studies of the metamorphic Aureole in Ghohroud Granitoid Intrusion Body*. (MSc dissertation). University of Isfahan, Isfahan, Iran (in Persian).

Ahmadi, T., & Posht Kuhi, M. (1993). Geochemisty and petrogenesis of Urumiah-Dokhtar volcanics around Nain and Rafsanjan areas: A preliminary study. *Treatise on the Geology of Iran. Iranian Ministry of Mines and Metals*,p. 90. Tehran: Geological Survey of Iran.

Alavi, M. (1991). *Tectonic map of the Middle East, scale 1:5 000 000*. Tehran: Geological Survey of Iran.

Alavi, M. (1994). Tectonics of the Zagros orogenic belt of Iran: New data and interpretations. *Tectonophysics*, *229*, 211–238. https://doi.org/10.1016/0040-1951(94)90030-2.

Alavi, M. (2004). Regional stratigraphy of the Zagros fold-thrust belt of Iran and its proforeland evolution. *American Journal of Science*, *304*, 1–20. https://doi.org/10.2475/ajs.304.1.1.

Alavi, M. (2007). Structures of the Zagros fold-thrust belt in Iran. *American Journal of Science*, *307*, 1064–1095. https://doi.org/10.2475/09.2007.02.

Allègre, C. J., & Minster, J. F. (1978). Quantitative models of trace element behavior in magmatic processes. *Earth and Planetary Science Letters*, *38*, 1–25.

Allen, M., Jackson, J., & Walker, R. (2004). Late Cenozoic reorganization of the Arabia-Eurasia collision and the comparison of short-term and long-term deformation rates. *Tectonics*, *23*, TC2008. https://doi.org/10.1029/2003TC001530.

Altherr, R., Holl, A., & Hegner, E. (2000). High-potassium, calc-alkaline I-type plutonism in the European Variscides: Northern Vosges (France) and northern Schwarzwald (Germany). *Lithos*, *50*, 51–73.

Amidi, S. M., Emami, M. H., & Michel, R. (1984). Alkaline character of Eocene volcanism in the middle part of central Iran and its geodynamic situation. *Geologische Rundschau*, *73*, 917–932. https://doi.org/10.1007/BF01820882.

Amidi, S. M., & Michel, R. (1985). Cenozoic magmatism of the Surk area (central Iran) stratigraphy, petrography, geochemistry and their geodynamic implications. *Géologie Alpine*, *61*, 1–16.

Anderson, T. (2002). Correction of common lead in U–Pb analyses that do not report 204Pb. *Chemical Geology*, *192*, 59–79. https://doi.org/10.1016/S0009-2541(02)00195-X.

Arvin, M., Pan, Y., Dargahi, S., Malekizadeh, A., & Babaei, A. (2007). Petrochemistry of the Siah-Kuh granitoid stock southwest of Kerman, Iran: Implications for initiation of Neotethys subduction. *Journal of Asian Earth Sciences*, *30*, 474–489. https://doi.org/10.1016/j.jseaes.2007.01.001.

Asadi, S. (2018). Triggers for the generation of post–collisional porphyry Cu systems in the Kerman magmatic copper belt, Iran: New constraints from elemental and isotopic (Sr–Nd–Hf–O) data. *Gondwana Research*, *64*, 97–121.

Ayati, F., Yavuz, F., Asadi, H. H., Richards, J. P., & Jourdan, F. (2013). Petrology and geochemistry of calc-alkaline volcanic and subvolcanic rocks, Dalli porphyry copper gold deposit, Markazi Province, Iran. *International Geology Review*, *55*, 158–184.

Azizi, H., Chung, S. L., Tanaka, T., & Asahara, Y. (2011). Isotopic dating of the Khoy Metamorphic Complex (KMC), northwestern Iran: A significant revision of the formation age and magma source. *Precambrian Research*, *185*, 87–94. https://doi.org/10.1016/j.precamres.2010.12.004.

Babazadeh, S., Ghorbani, M. R., Broker, M., D'Antonio, M., Cottle, J., Gebbing, T., … Ahmadi, P. (2017). Late Oligocene–Miocene mantle upwelling and interaction inferred from mantle signatures in gabbroic to granitic rocks from the Urumieh–Dokhtar arc, south Ardestan, Iran. *International Geology Review*, *59*, 1938–2839. https://doi.org/10.1080/00206814.2017.1286613.

Ban, M., Takahashi, K., Horie, T., & Toya, N. (2005). Petrogenesis of mafic inclusions in rhyolitic lavas from Narugo Volcano, Northeastern Japan. *Journal of Petrology*, *46*, 1543–1563.

Barbarin, B. (1990). Plagioclase xenocrysts and mafic magmatic enclaves in some granitoids of the Sierra Nevada batholith, California. *Journal of Geophysical Research*, *95*, 17747–17756.

Barbarin, B. (1999). A review of the relationship between granitoid types, their origins and their geodynamic environments. *Lithos*, *46*, 605–626.

Barbarin, B. (2005). Mafic magmatic enclaves and mafic rocks associated with some granitoids of the central Sierra Nevada batholith, California: Nature, origin, and relations with the hosts. *Lithos*, *80*, 155–177.

Ben Othman, D., Fourcade, S., & Allegre, C. J. (1984). Recycling processes in granite-granodiorite genesis: The Querigut case studied by Nd–Sr isotope systematics. *Earth and Planetary Science Letters*, *69*, 290–300.

Berberian, F., & Berberian, M. (1981). Tectono-plutonic episodes in Iran. In H. K. Gupta & F. M. Delany (Eds.), *Zagros-Hindu Kush–Himalaya geodynamic evolution* (Vol. 3, pp. 5–32). Washington DC: American Geophysical Union.

Berberian, F., Muir, I. D., Pankhurst, R. J., & Berberian, M. (1982). Late Cretaceous and Early Miocene Andean-type plutonic activity in northern Makran and Central Iran. *Journal of Geological Society London*, *139*, 605–614. https://doi.org/10.1144/gsjgs.139.5.0605.

Berberian, M., & King, G. C. P. (1981). Towards a paleogeography and tectonic evolution of Iran. *Canadian Journal of Earth Sciences*, *18*, 210–265. https://doi.org/10.1139/e81-019.

Bonev, N., Dilek, Y., Hanchar, J. M., Bogdanov, K., & Klain, L. (2011). Nd–Sr–Pb isotopic composition and mantle sources of Triassic rift units in the Serbo-Macedonian and the western Rhodope Massifs (Bulgaria–Greece). *Geological Magazine*, *149*, 146–152. https://doi.org/10.1017/S0016756811000938.

Bonin, B. (2004). Do coeval mafic and felsic magmas in post-collisional to within-plate regimes necessarily imply two constrasting, mantle and crust, sources? A review. *Lithos*, *78*, 1–24.

Brown, G. C., Thorpe, R. S., & Webb, P. C. (1984). The geochemical characteristics of granitoids in contrasting arcs and comments on magma sources. *Journal of the Geological Society*, *141*(3), 413–426. https://doi.org/10.1144/gsjgs.141.3.0413.

Cameron, B. I., Walker, J. A., Carr, M. J., Patino, L. C., Matias, O., & Feigenson, M. D. (2003). Flux versus decompression melting at stratovolcanos in southeastern Guatemala. *Journal of Volcanology and Geothermal Research*, *119*, 21–50.

Chappell, B. J., & White, A. J. R. (1974). Two contrasting granite types. *Pacific Geology*, *8*, 173–174.

Chappell, B. W. (1996). Magma mixing and the production of compositional variation within granite suites: Evidence from the granites of southeastern Australia. *Journal of Petrology*, *37*, 449–470.

Chappell, B. W., White, A. J. R., & Wyborn, D. (1987). The importance of residual source material (restite) in granite petrogenesis. *Journal of Petrology*, *28*, 1111–1138.

Chen, C. J., Chen, B., Li, Z., & Wang, Z. Q. (2016). Important role of magma mixing in generating the Mesozoic monzodioritic–granodioritic intrusions related to Cu mineralization, Tongling, East China: Evidence from petrological and in situ Sr-Hf isotopic data. *Lithos*, *248*, 80–93.

Chen, F., Li, X. H., Wang, X. L., Li, Q. L., & Siebel, W. (2007). Zircon age and Nd-Hf isotopic composition of the Yunnan Tethyan belt, southwestern China. *International Journal of Earth Sciences*, *96*, 1179–1194.

Chiu, H.-Y., Chung, S.-L., Zarrinkoub, M. H., Mohammadi, S. S., Khatib, M. M., & Iizuka, Y. (2013). Zircon U-Pb age constraints from Iran on the magmatic evolution related to Neotethyan subduction and Zagros orogeny. *Lithos*, *162-163*, 70–87. https://doi.org/10.1016/j.lithos.2013.01.006.

Christiansen, E. H., & Keith, J. D. (1996). Trace element systematics in silicic magmas: a metallogenic perspective. In D. A. Wyman (Ed.), *Trace element geochemistry of volcanic rocks: Applications for massive sulfide exploration* (pp. 115–151). Geological Association of Canada, Short Course Notes, 12.

Clynne, M. A. (1999). A complex magma mixing origin for rocks erupted in 1915, Lassen peak, California. *Journal of Petrology*, *40*, 105–132.

Dargahi, S. (2007). *Post-collisional Miocene magmatism in the Sarcheshmeh-Shahrebabak region, NW of Kerman: Isotopic study, petrogenetic analysis and geodynamic pattern of granitoid intrusives and the role of adakitic magmatism in development of copper mineralization*. (Unpublished PhD thesis). Shahid Bahonar University of Kerman, (p. 310) (in Persian).

Dargahi, S., Arvin, M., Pan, Y., & Babaei, A. (2010). Petrogenesis of post-collisional a-type granitoids from the Urumieh–Dokhtar magmatic assemblage, southwestern Kerman, Iran: Constraints on the Arabian–Eurasian continental collision. *Lithos*, *115*, 190–204. https://doi.org/10.1016/j.lithos.2009.12.002.

De La Roche, H., Leterrier, J., Grande Claude, P., & Marchal, M. (1980). A classification of volcanic and plutonic rocks using R1R2-diagrams and major-element analyses—its relationship and current nomenclature. *Chemical Geology*, *29*, 183–210. https://doi.org/10.1016/0009-2541(80)90020-0

DePaolo, D. J. (1981). Trace element and isotopic effects of combined wall rock assimilation and fractional crystallization. *Earth and Planetary Science Letters*, *53*, 189–202. https://doi.org/10.1016/0012-821X(81)90153-9.

Dercourt, J., Zonenshain, L. P., Ricou, L. E., Kazmin, V. G., Le Pichon, X., Knipper, A. L., … Laver, J. (1986). Geological evolution of the Tethys belt from the Atlantic to the Pamirs since the Lias. *Tectonophysics*, *123*, 241–315.

Dewey, J. F., Pitman, W. C., Ryan, W. B. F., & Bonnin, J. (1973). Plate tectonics and the evolution of the Alpine System. *GSA Bulletin*, *84*(10), 3137–3180.

Didier, J. (1973). Granites and Their Enclaves: The bearing of enclaves on the origin of granites. *Developments in Petrology*, p.393. Amsterdam: Elsevier.

Didier, J. (1991). The various types of enclaves in the Hercynian granitoids of the Massif Central, France. In J. Didier & B. Barbarin (Eds.), *Enclaves and granite petrology*, p. 47-61, Amesterdam: Elsevier.

Didier, J., & Barbarin, B. (1991). *Enclaves and granite petrology: Developments in petrology*, *13*. Amsterdam: Elsevier.

Dilek, Y., Imamverdiyev, N., & Altunkaynak, S. (2010). Geochemistry and tectonics of Cenozoic volcanism in the Lesser Caucasus (Azerbaijan) and the peri-Arabian region: Collision-induced mantle dynamics and its magmatic fingerprint. *International Geology Review*, *52*, 536–578. https://doi.org/10.1080/00206810903360422.

Eichelberger, J. C., Cherkoff, D. G., Dreher, S. T., & Nye, C. J. (2000). Magmas in collision: Rethinking chemical zonation in silicic magmas. *Geology*, *28*, 603–606.

Emami, M. H. (1981). *Geological quadrangle map of Iran, 1:250,000 scale, sheet E6 (Qom)*. Geological Survey of Iran.

Fang, Y., Zhang, Y., Zhang, S., Cao, H., Zou, H., & Dong, J. (2017). Early Cretaceous I-type granites in the Tengchong terrane: New constraints on the Late Mesozoic tectonic evolution of southwestern China. *Geoscience Frontiers.*, *9*, 459–470. https://doi.org/10.1016/j.gsf.2017.04.007.

Fernández, C., & Castro, A. (2018). Mechanical and structural consequences of magma differentiation at ascent conduits: A possible origin for some mafic microgranular enclaves in granites. *Lithos*, *320–321*, 49–61.

Foley, S., Tiepolo, M., & Riccardo, V. (2002). Growth of early continental crust controlled by melting of amphibolite in subduction zones. *Nature*, *417*, 837–840.

Fourcade, S., & Javoy, M. (1991). Sr-Nd-O isotopic features of mafic microgranular enclaves and host granitoids from the Pyrenees, France: Evidence for their hybrid nature and inference on their origin. In J. Didier & B. Barbarin (Eds.), *Enclaves and granite petrology. Developments in petrology* (Vol. 13, pp. 345–364). Amsterdam: Elsevier.

Gharamohammadi, Z., & Kananian, A. (2016). Geochemistry and petrogenesis of the Dehe Bala calc-alkaline granodiorites, south west of Boein Zahra. *Iranian Journal of Petrology*, *7*, 147–170 (In Persian with English abstract).

Ghasemi, A., & Tabatabaei Manesh, S. M. (2015). Geochemistry and petrogenesis of Ghohroud Igneous Complex (Urumieh–Dokhtar zone): Evidence for Neotethyan subduction during the Neogene. *Arabian Journal of Geosciences*, *8*, 9599–9623. https://doi.org/10.1007/s12517-015-1883-7.

Ghorbani, M. R. (2006). Lead enrichment in Neotethyan volcanic rocks from Iran: The implications of a descending slab. *Geochemical Journal*, *40*, 557–568. https://doi.org/10.2343/geochemj.40.557.

Ghorbani, M. R., & Bezenjani, R. N. (2011). Slab partial melts from the metasomatizing agent to adakite, Tafresh Eocene volcanic rocks, Iran. *Island Arc*, *20*, 188–202.

Ghorbani, M. R., Graham, I. T., & Ghaderi, M. (2014). Oligocene–Miocene geodynamic evolution of the central part of Urumieh-Dokhtar Arc of Iran. *International Geology Review*, *56*, 1039–1050. https://doi.org/10.1080/00206814.2014.919615.

Gorton, M. P., & Schandl, E. S. (2000). From continents to Island arcs: A geochemical index of tectonic setting for arc-related and within-plate felsic to intermediate volcanic rocks. *The Canadian Mineralogist*, *38*, 1065–1073.

Haghipour, A., & Aghanabati, A. (1985). *Geologic map of Iran: Ministry of mines and metals, one plate, scale 1:2,500,000*. Tehran: Geological Survey of Iran.

Hart, S. R. (1984). A large-scale isotope anomaly in the Southern Hemisphere mantle. *Nature*, *309*, 753–757.

Haschke, M., Ahmadian, J., Murata, M., & McDonald, I. (2010). Copper mineralization prevented by arc-root delamination during Alpine–Himalayan collision in central Iran. *Economic Geology*, *105*, 855–865.

Hassanzadeh, J., Stockli, D. F., Horton, B. K., Axen, G. J., Stockli, L. D., Grove, M., … Walker, J. D. (2008). U–Pb zircon geochronology of late Neoproterozoic–Early Cambrian granitoids in Iran: Implications for paleogeography, magmatism, and exhumation history of Iranian basement. *Tectonophysics*, *451*, 71–96. https://doi.org/10.1016/j.tecto.2007.11.062.

Hibbard, M. J. (1991). Textural anatomy of twelve magma-mixed granitoid systems. In J. Didier & B. Barbarin (Eds.), *Enclaves and granite petrology. Developments in petrology* (pp. 431–444). Amsterdam: Elsevier.

Hofmann, A. W. (1988). Chemical differentiation of the Earth: The relationship between mantle, continental crust and oceanic crust. *Earth and Planetary Science Letters*, *90*, 297–314.

Honarmand, M., Rashidnejad Omran, N., Corfu, F., Emami, M. H., & Nabatian, G. (2013). Geochronology and magmatic history of a calc-alkaline plutonic complex in the Urumieh-Dokhtar Magmatic Belt,

Central Iran: Zircon ages as evidence for two major plutonic episodes. *Neues Jahrbuch fur Mineralogie—Abhandlungen*, *190*, 67–77. https://doi.org/10.1127/0077-7757/2013/0230.

Honarmand, M., Rashidnejad Omran, N., Neubauer, F., Hashem Emami, M., Nabatian, G., Liu, X., … Chen, B. (2014). Laser-ICP-MS U-Pb zircon ages and geochemical and Sr–Nd–Pb isotopic compositions of the Niyasar plutonic complex, Iran: Constraints on petrogenesis and tectonic evolution. *International Geology Review*, *56*, 104–132. https://doi.org/10.1080/00206814.2013.820375.

Hou, Z., Zhang, H., Pan, X., & Yang, Z. (2011). Porphyry Cu (-Mo-Au) deposits related to melting of thickened mafic lower crust: Examples from the eastern Tethyan metallogenic domain. *Ore Geology Reviews*, *39*, 21–45. https://doi.org/10.1016/j.oregeorev.2010.09.002.

Irvine, T. N., & Baragar, W. R. A. (1971). A Guide to the chemical classification of the common volcanic rocks. *Canadian Journal of Earth Sciences*, *8*, 523–548. https://doi.org/10.1139/e71-055.

Jung, D., Kursten, M., & Tarkian, M. (1976). Post-mesozoic volcanism in Iran and its relation to the subduction of the Afro-Arabian under the Eurasian plate. In A. Pilger & A. Rosler (Eds.), *Afar between continental and oceanic rifting* (pp. 175–181). Stuttgart: Schweizerbartsche Verlagbuchhandlung.

Kananian, A., Sarjoughian, F., Nadimi, A., Ahmadian, J., & Ling, W. (2014). Geochemical characteristics of the Kuh-e Dom intrusion, Urumieh–Dokhtar Magmatic Arc (Iran): Implications for source regions and magmatic evolution. *Journal of Asian Earth Sciences*, *90*, 137–148. https://doi.org/10.1016/j.jseaes.2014.04.026.

Karsli, O., Dokuz, A., Uysal, I., Aydin, F., Chen, B., Kandemir, R., & Wijbrans, J. (2010). Relative contributions of crust and mantle to generation of Campanian high-K calc-alkaline I-type granitoids in a subduction setting, with special reference to the Harsit Pluton, Eastern Turkey. *Contributions to Mineralogy and Petrology*, *160*, 467–487.

Kazemi, K., Kananian, A., Xiao, Y., & Sarjoughian, F. (2018). Petrogenesis of Middle-Eocene granitoids and their mafic microgranular enclaves in central Urmia-Dokhtar Magmatic Arc (Iran): Evidence for interaction between felsic and mafic magmas. *Geoscience Frontiers*, *10*, 705–723.

Kemp, A. I. S., Hawkesworth, C. J., Foster, G. L., Paterson, B. A., Woodhead, J. D., Hergt, J. M., … Whitehouse, M. J. (2007). Magmatic and crustal differentiation history of granitic rocks from H-O isotopes in zircon. *Science*, *315*, 980–983.

Khaksar, T., Rashidnejad-Omran, N., Chen, F., Song, S. G., Li, S. Q., & Ghaderi, M. (2020). Zircon U-Pb ages and magmatic history of the Kashan Plutons in the Central Urumieh-Dokhtar Magmatic Arc, Iran: Evidence for Neotethyan subduction during Paleogene-Neogene. *Journal of Earth Science*, *31*(1), 53–68.

Kumar, S., & Rino, V. (2006). Mineralogy and geochemistry of microgranular enclaves in Palaeoproterozoic Malanjkhand granitoids, central India: Evidence of magma mixing, mingling, and chemical equilibration. *Contributions to Mineralogy and Petrology*, *152*, 591–609.

Lowell, G. R., & Young, G. J. (1999). Interaction between coeval mafic and felsic melts in the St. Francois Terrane of Missouri, USA. *Precambrian Research*, *95*, 69–88.

Ludwig, K. R. (2003). *Isoplot V. 3.0: A geochronological toolkit for Microsoft Excel* (p. 70). Berkeley: Berkeley Geochronology Center Special Publication 4.

Maas, R., Kinny, P. D., Williams, I. S., Froude, D. O., & Compston, W. (1992). The Earth's oldest known crust: A geochronological and geochemical study of 3900–4200 Ma old detrital zircons from Mt. Narryer and Jack Hills, Western Australia. *Geochimica et Cosmochimica Acta*, *56*, 1281–1300. https://doi.org/10.1016/0016-7037(92)90062-N.

McClusky, S., Reilinger, R., Mahmoud, S., Ben Sari, D., & Tealeb, A. (2003). GPS constraints on Africa (Nubia) and Arabia plate motions. *Geophysical Journal International*, *155*, 126–138. https://doi.org/10.1046/j.1365-246X.2003.02023.x.

Middlemost, E. A. K. (1994). Naming materials in the magma/igneous rock system. *Earth-Science Reviews*, *37*, 215–224.

Moghadam, H., Rossetti, F., Lucci, F., Chiaradia, M., Gerdes, A., Martinez, M. L., … Nasrabady, M. (2016). The calc-alkaline and adakitic volcanism of the Sabzevarstructural zone (NE Iran): Implications for the Eocene magmatic flare-up in Central Iran. *Lithos*, *248*, 517–535. https://doi.org/10.1016/j.lithos.2016.01.019.

Moghadam, H. S., & Stern, R. J. (2011). Geodynamic evolution of Upper Cretaceous Zagros ophiolites: Formation of oceanic lithosphere above a nascent subduction zone. *Geological Magazine*, *148*, 762–801. https://doi.org/10.1017/S0016756811000410.

Mohajjel, M., & Fergusson, C. (2000). Dextral transpression in Late Cretaceous continental collision, Sanandaj–Sirjan zone, western Iran. *Journal of Structural Geology*, *22*, 1125–1139. https://doi.org/10.1016/S0191-8141(00)00023-7.

Mohajjel, M., Fergusson, C., & Sahandi, M. (2003). Cretaceous-Tertiary convergence and continental collision, Sanandaj-Sirjan Zone, western Iran. *Journal of Asian Earth Sciences*, *21*, 397–412. https://doi.org/10.1016/S1367-9120(02)00035-4.

Mohajjel, M., & Fergusson, C. L. (2014). Jurassic to Cenozoic tectonics of the Zagros Orogen in northwestern Iran. *International Geology Review*, *56*, 263–287.

Moinvaziri, H. (1985). *Volcanisme Tertiaire et Quaternaire en Iran*. (PhD dissertation). Orsay, Paris-Sud, France (p. 290) (in French).

Müller, D., & Groves, D. I. (1997). *Potassic igneous rocks and associated gold-copper mineralization*. Lecture Notes in Earth Sciences 238. No. 56.

Nakamura, N. (1974). Determination of REE, Ba, Fe, Mg, Na and K in carbonaceous and ordinary chondrites. *Geochimica et Cosmochimica Acta*, *38*, 757–775. https://doi.org/10.1016/0016-7037(74)90149-5.

Omrani, J., Agard, P., Whitechurch, H., Benoit, M., Prouteau, G., & Jolivet, L. (2008). Arc magmatism and subduction history beneath the Zagros Mountains, Iran: A new report of adakites and geodynamic consequences. *Lithos*, *106*, 380–398. https://doi.org/10.1016/j.lithos.2008.09.008.

Patino-Douce, A. E. (1999). What do experiments tell us about the relative contributions of crust and mantle to the origin of granitic magmas? In A. Castro, C. Fernandez, & J. L. Vigneresse (Eds.), *Understanding granites: Integrating new and classical techniques* (pp. 55–75). London, Special Publications 168: Geological Society. https://doi.org/10.1144/GSL.SP.1999.168.01.05.

Pearce, J. (1996). Source and settings of granitic rocks. *Episodes*, *19*, 120–125.

Pearce, J. A., Harris, N. B. W., & Tindle, A. G. (1984). Trace element discrimination diagrams for the tectonic interpretation of granitic rocks. *Journal of Petrology*, *25*, 956–983. https://doi.org/10.1093/petrology/25.4.95.

Perugini, D., Poli, G., Christofides, G., & Eleftheriadis, G. (2003). Magma mixing in the Sithonia Plutonic Complex, Greece: Evidence from mafic microgranular enclaves. *Mineralogy and Petrology*, *78*, 173–200. https://doi.org/10.1007/s00710-002-0225-0.

Radfar, J. (1993). *Explanatory text of Kashan*. Geological quadrangle map 1: 100000, No. 6257. Geological Survey of Iran (in Persian).

Rapp, R. P., & Watson, E. B. (1995). Dehydration melting of metabasalt at 8-32 kbar: Implications for continental growth and crust-mantle recycling. *Journal of Petrology*, *36*, 891–931. https://doi.org/10.1093/petrology/36.4.891.

Rapp, R. P., Watson, E. B., & Miller, C. F. (1991). Partial melting of amphibolite/eclogite and the origin of Archean trondhjemites and tonalites. *Precambrian Research*, *51*, 1–25.

Rezaei-Kahkhaei, M., Galindo, G., Pankhurst, R. J., & Esmaeily, D. (2011). Magmatic differentiation in the calc-alkaline Khalkhab Neshveh pluton, Central Iran. *Journal of Asian Earth Sciences*, *42*, 499–514.

Rollinson, H. R. (1993). *Using geochemical data: Evaluation, presentation, and interpretation* (p. 352). Harlow: Longman.

Rottura, A., Bargossi, G. M., Caggianelli, A., Del Moro, A., Visona, D., & Tranne, C. A. (1998). Origin and significance of the Permian high-K calc-alkaline magmatism in the central-eastern Southern Alps, Italy. *Lithos*, *45*, 329–348. https://doi.org/10.1016/S0024-4937(98)00038-3.

Rudnick, R. L. (1992). Xenoliths—Examples of the lower crust. In D. M. Fountain, R. Arculus, & R. W. Kay (Eds.), *Continental lower crust* (pp. 269–316). Amsterdam: Elsevier.

Rudnick, R. L., & Fountain, D. M. (1995). Nature and composition of the continental crust: A lower crustal perspective. *Reviews of Geophysics*, *33*, 267–309.

Safaei, H., Taheri, A., & Vaziri-Moghaddam, H. (2008). Structural Analysis and Evolution of the Kashan (Qom-Zefreh) Fault, Central Iran. *Journal of Applied Science*, *8*, 1426–1434.

Sarjoughian, F., Kananian, A., Haschke, M., Ahmadian, J., Ling, W., & Zong, K. (2012). Magma mingling and hybridization in the Kuh-e Dom pluton, Central Iran. *Journal of Asian Earth Sciences*, *54-55*, 49–63. https://doi.org/10.1016/j.jseaes.2012.03.013.

Sarjoughian, F., Lentz, D., Kananian, A., Ao, S., & Xiao, W. (2018). Geochemical and isotopic constraints on the role of juvenile crust and magma mixing in the UDMA magmatism, Iran: Evidence from mafic microgranular enclaves and cogenetic granitoids in the Zafarghand igneous complex. *Earth Science*, *107*, 1127–1151.

Schiano, P., Monzier, M., Eissen, J. P., Martin, H., & Koga, K. T. (2010). Simple mixing as the major control of the evolution of volcanic suites in the Ecuadorian Andes. *Contributions to Mineralogy and Petrology*, *160*, 297–312.

Sen, P. A., Temel, A., & Gourgaud, A. (2004). Petrogenetic modelling of Quaternary post-collisional volcanism: A case study of central and eastern Anatolia. *Geological Magazine*, *141*, 81–98. https://doi.org/10.1017/S0016756803008550.

Sepahi, A. A., & Athari, S. F. (2006). Petrology of major granitic plutons of the northwestern part of the Sanandaj-Sirjan Metamorphic Belt, Zagros Orogen, Iran: With emphasis on A-Type granitoids from the SE Saqqez Area. *Neues Jahrbuch Fur Mineralogie-Abhandlungen*, *183*, 93–106.

Sepidbar, F., Moghadam, H. S., Zhang, L., Li, J. W., Ma, J., Stern, R. J., & Lin, C. (2019). Across-arc geochemical variations in the Paleogene magmatic belt of Iran. *Lithos*, *344*, 280–296.

Shafaii Moghadam, H., Khademi, M., Hu, Z., Stern, R. J., Santos, J. F., & Wu, Y. (2015). Cadomian (Ediacarane–Cambrian) arc magmatism in the ChahJam–Biarjmand metamorphic complex (Iran): Magmatism along the northern active margin of Gondwana. *Gondwana Research*, *27*, 439–452.

Shahabpour, J. (2007). Island-arc affinity of the Central Iranian Volcanic Belt. *Journal of Asian Earth Sciences*, *30*, 652–665. https://doi.org/10.1016/j.jseaes.2007.02.004

Shahbazi, H., Siebel, W., Pourmoafee, M., Ghorbani, M., Sepahi, A. A., Shang, C. K., & Abedini, M. V. (2010). Geochemistry and U-Pb zircon geochronology of the Alvand Plutonic Complex in Sanandaj-Sirjan Zone (Iran): New evidence for Jurassic magmatism. *Journal of Asian Earth Sciences*, *39*, 668–683. https://doi.org/10.1016/j.jseaes.2010.04.014.

Shahsavari Alavijeh, B., Rashidnejad-Omran, N., & Corfu, F. (2017). Zircon U-Pb ages and emplacement history of the Nodoushan Plutonic Complex in the Central Urumieh-Dokhtar Magmatic Belt, Central Iran: Product of Neotethyan subduction during the Paleogene. *Journal of Asian Earth Sciences*, *143*, 283–295. https://doi.org/10.1016/j.jseaes.2017.03.034.

Shand, S. J. (1943). *Eruptive rocks* (2nd ed.). New York, NY: John Wiley.

Shellnutt, J. G., Wang, C. Y., Zhou, M. F., & Yang, Y. (2009). Zircon Lu-Hf isotopic compositions of metaluminous and peralkaline A-type granitic plutons of the Emeishan large igneous province (SW China): Constraints on the mantle source. *Journal of Asian Earth Sciences*, *35*, 45–55.

Silva, L. C., Hartmann, L. A., McNaughton, N. J., & Fletcher, I. R. (2000). Zircon U-Pb SHRIMP dating of a Neoproterozoic overprint in a Paleoproterozoic granitic-gneissic complex, southernmost Brazil. *American Mineralogist*, *85*, 649–667.

Song, S. G., Niu, Y. L., Wei, C. J., Ji, J. Q., & Su, L. (2010). Metamorphism, anatexis, zircon ages and tectonic evolution of the Gongshan block in the northern Indochina continent—An eastern extension of the Lhasa Block. *Lithos*, *120*, 327–346.

Stephens, W. E., Holden, P., & Henney, J. (1991). Microdiorite enclaves within the Scottish Caledonian granitoids and their significance for crustal magmatism. In J. Didier & B. Barbarin (Eds.), *Enclaves and granite petrology. Developments in petrology* (Vol. 13, pp. 125–134). Amsterdam: Elsevier.

Stöcklin, J. (1968). Structural history and tectonics of Iran: A review. *American Association of Petroleum Geologists Bulletin*, *52*, 1229–1258. https://doi.org/10.1306/5D25C4A5-16C1-11D7-8645000102C1865D.

Streckeisen, A. L. (1976). To each plutonic rock its proper name. *Earth Science Reviews*, *12*, 1–33.

Sun, S. J., Zhang, R. Q., Cong, Y. N., Zhang, L. P., Sun, W. D., Li, C. Y., & Ding, X. (2020). Analogous diagenetic conditions of dark enclave and its host granite derived by magma mixing: Evidence for a post-mixing magmatic process. *Lithos*, *356–357*, 105373. https://doi.org/10.1016/j.lithos.2020.105373.

Sun, S. S., & McDonough, W. F. (1989). Chemical and isotopic systematics of oceanic basalts: Implications for mantle composition and processes. In A. D. Saunders & M. J. Norry (Eds.), *Magmatism in ocean basins* (pp. 313–345). London Special Publication 42: Geological Society of London. https://doi.org/10.1144/GSL.SP.1989.042.01.19.

Taylor, S. R., & McLennan, S. M. (1985). *The continental crust: Its composition and evolution* (p. 312). Carlton: Blackwell Scientific Publication.

Verdel, C., Wernicke, B. P., Hassanzadeh, J., & Guest, B. (2011). A Paleogene extensional arc flare-up in Iran. *Tectonics*, *30*, 1–20. https://doi.org/10.1029/2010TC002809.

Vernon, R. H. (1984). Microgranitoid enclaves in granites-globules of hybrid magma quenched in a plutonic environment. *Nature*, *309*, 438–439.

Vernon, R. H. (2014). Microstructures of microgranitoid enclaves and the origin of S-type granitoids. *Australian Journal of Earth Sciences*, *61*, 227–239.

Waight, T. E., Maas, R., & Nicholls, I. A. (2000). Fingerprinting feldspar phenocrysts using crystal isotopic composition stratigraphy: Implications for crystal transfer and magma mingling in S-type granites. *Contributions to Mineralogy and Petrology*, *139*, 227–239. https://doi.org/10.1007/s004100000128.

Wang, Q., Xu, J. F., Zhao, Z. H., Xiong, X. L., Bao, Z. W., Xu, W., & Xiong, X. L. (2004). Cretaceous high-potassium intrusive rocks in the Yueshan-Hongzhen area of east China: Adakites in an extensional tectonic regime within a continent. *Geochemical Journal*, *38*, 417–434.

Weaver, B. L., & Tarney, J. (1984). Empirical approach to estimating the composition of the continental crust. *Nature*, *310*, 575–577.

Wedepohl, K. H. (1995). The composition of the continental crust. *Geochimica et Cosmochimica Acta*, *59*, 1217–1232.

Wiedenbeck, M., Alle, P., Corfu, F., Griffin, W. L., Meier, M., Oberli, F., … Spiegel, W. (1995). Three natural zircon standards for U-Th-Pb, Lu- Hf, trace element and REE analyses. *Geostandand Newsletter*, *19*, 1–23. https://doi.org/10.1111/j.1751-908X.1995.tb00147.x.

Xu, J. F., Shinjo, R., Defant, M. J., Wang, Q., & Rapp, R. P. (2002). Origin of Mesozoic adakitic intrusive rocks in the Ningzhen area of east China: Partial melting of delaminated lower continental crust. *Geology*, *30*, 1111–1114.

Yang, H., Ge, W., Zhao, G., Dong, Y., Xu, W. L., Ji, Z., & Yu, J. (2015). Late Triassic intrusive complex in the Jidong region, JiamusieKhanka Block, NE China: Geochemistry, zircon U-Pb ages, Lu-Hf isotopes, and implications for magma mingling and mixing. *Lithos*, *224-225*, 143–159.

Yang, J. H., Wu, F. Y., Chung, S. L., Wilde, S. A., & Chu, M. F. (2004). Multiple sources for the origin of granites: Geochemical and Nd/Sr isotopic

evidence from the Gudaoling granite and its mafic enclaves, NE China. *Geochimica et Cosmochimica Acta*, *68*, 4469–4483.

Yang, J. H., Wu, F. Y., Chung, S. L., Wilde, S. A., & Chu, M. F. (2006). A hybrid origin for the Qianshan A-type granite, northeast China: Geochemical and Sr-Nd-Hf isotopic evidence. *Lithos*, *89*, 89–106.

Yeganehfar, H., Ghorbani, M. R., Shinjo, R., & Ghaderi, M. (2013). Magmatic and geodynamic evolution of Urumieh–Dokhtar basic volcanism, Central Iran: Major, trace element, isotopic, and geochronologic implications. *International Geology Review*, *55*(6), 767–786.

Zhao, J., Zhong, D. L., & Wang, Y. (1994). Meta-morphism of Lancang Metamorphic Belt, the western Yunnan and its relation and deformation. *Acta Petrologica Sinica*, *10*(1), 27–40 (in Chinese with English abstract).

Zindler, A., & Hart, S. R. (1986). Chemical geodynamics. *Annual Review of Earth and Planetary Sciences*, *14*, 493–571. https://doi.org/10.1146/annurev.ea.14.050186.002425.

SUPPORTING INFORMATION

Additional supporting information may be found in the online version of the article at the publisher's website.

How to cite this article: Khaksar, T., Rashidnejad-Omran, N., Li, S.-Q., Song, S.-G., Kananian, A., Chen, F., & Li, S. (2022). Geochronology and petrogenesis of granitoids and associated mafic enclaves from Ghohroud in the Urumieh–Dokhtar Magmatic Arc (Iran): Evidence for magma mixing during the closure of the Neotethyan Ocean. *Geological Journal*, *57*(8), 3313–3332. https://doi.org/10.1002/gj.4480